Kanak, K. M., and J. M. Straka, 2023: Observational study of two Norman, Oklahoma storms with very large, damaging hail in long-hodograph environments. *Electronic J. Severe Storms Meteor.,* **18** (1), 1–41.

Electronic Journal of
SEVERE STORMS METEOROLOGY

Observational Study of Two Norman, Oklahoma Storms with Very Large, Damaging Hail in Long-Hodograph Environments

KATHARINE M. KANAK and JERRY M. STRAKA
Norman, Oklahoma

(Submitted 18 April 2023; in final form 20 November 2023)

ABSTRACT

Two ≥3-in (7.6-cm) hailstorms affected Norman, Oklahoma in 2021: one on 28–29 April and the other on 10–11 October. Wind-driven hail associated with the April storm was estimated to have caused over two million dollars in damage just to county-owned buildings, with estimates of hundreds of millions in damage when including privately owned properties. The October storm caused further damage in approximately the same locations in Norman as the April storm. That these storms affected Norman in a single year was unusual, as only three other prior dates had ≥3-in (7.6-cm) hail reports in Norman from 1955–2021. Radar presentations, surface and upper-air observations, and environmental parameters are presented and intercompared. The April storm was situated behind a surface boundary, and was mostly sub-severe until it rapidly intensified upon approach to the boundary, while the October storm evolved near a surface boundary and had a history of tornadoes. A cursory comparison of model-derived and observed proximity soundings for the two 2021 hailstorms with those for the previous six ≥3-in (7.6-cm) hailstorm dates for Cleveland County (in which Norman is located), from 1955–2021, showed that the two 2021 storms had lower environmental buoyancy, but larger deep shear. This study supports both: 1) the idea that large shear or buoyancy can compensate for lack of the other for the production of significant hail, and 2) the association of long hodographs with large-hail events.

1. Introduction

Central Oklahoma, in the south-central United States, is one of the more likely locations for significant hail (diameter ≥2 in or 5.1 cm; Hales 1988; Fig. 1a, Storm Prediction Center [SPC] 2023a) and hail with diameter ≥3 in (7.6 cm; Fig. 1b, adapted from Allen and Tippett 2015). Even so, the probable number of days per year within 25 mi (40.2 km) of a point in Cleveland County, OK (near the geographical center of Oklahoma) on which significant hail is likely to occur was 0.8–1.0 based on hail reports from 1986–2015 (Fig. 1a), and was even less for ≥3-in (7.6-cm) hail at 0.125–0.15 days per year (Fig. 1b). This equates to one 3-in (7.6–cm) hail day in 6.67–8 y or two in 13.33–16 y.

In 2021, two ≥3-in (7.6-cm) hailstorms affected Norman, OK, which is located within Cleveland County: one on 28–29 April (hereafter, the April storm) and one on 10–11 October (hereafter, the October storm). The occurrence of two ≥3-in (7.6-cm) hailstorm days within a single year (within 25 mi or 40.2 km or a point in central Oklahoma) is at least an order of magnitude less likely than might be expected based on Fig. 1b. The only other year in which there were also two ≥3-in (7.6-cm) hailstorms on different dates that affected Cleveland County was in 2010, but 2021 was the only year that there were two ≥3-in (7.6-cm) hail dates within the city limits of Norman. No years from 1955–2021 had more than two ≥3-in (7.6-cm) hailstorm dates for either Cleveland County or Norman.

Corresponding author address: Katharine M. Kanak, E-mail: katharinemkanak@gmail.com.

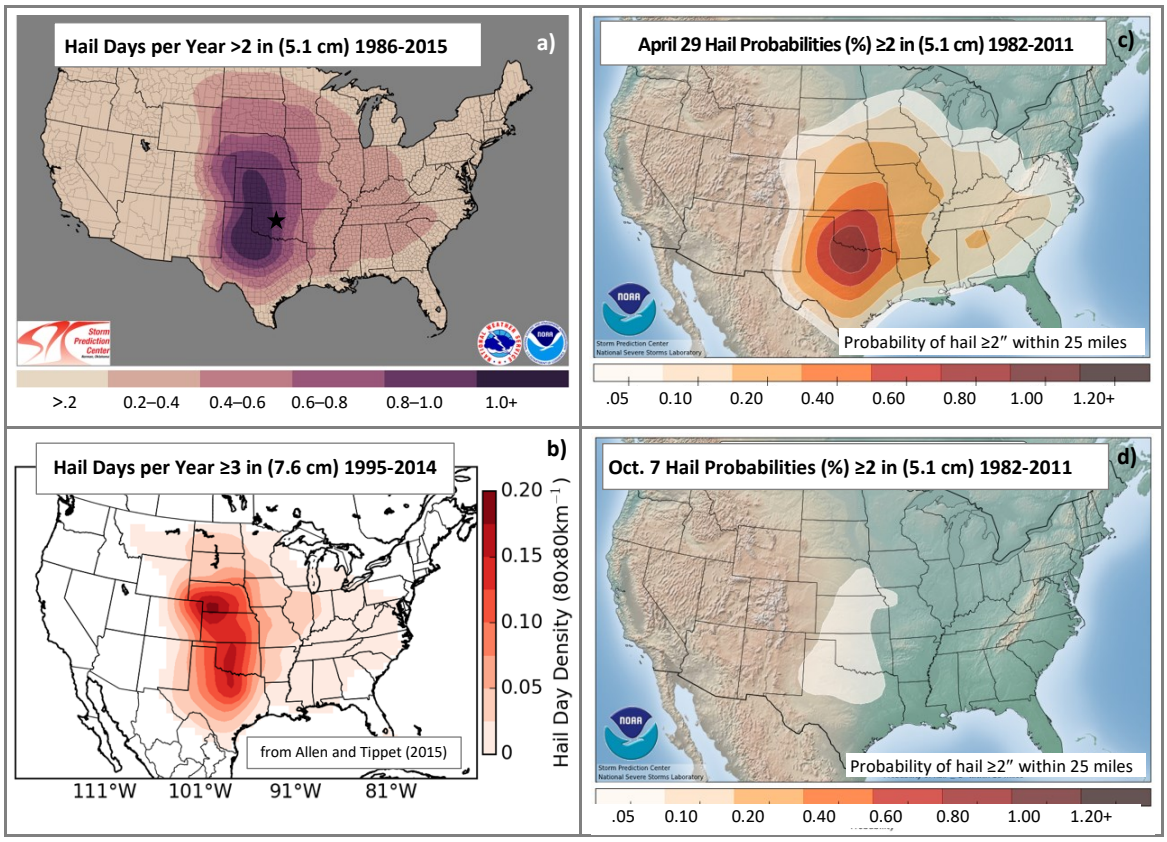

Figure 1: a) Mean annual frequency of >2-in (5.1-cm) hail days per year within 25 mi (40.2 km) of a point based on data from 1986–2015 (SPC 2023a). The black star in (a) denotes Cleveland County, OK. b) (from Allen and Tippett, 2015, their Fig. 9h). Mean hail days per year for ≥3-in (7.6-cm) hail from 1995–2014. Shading shows the Gaussian-kernel-smoothed, hail-day density (80 × 80 km^{-1}). c) and d) Significant hail (≥2 in or 5.1 cm) probabilities within 25 mi (40.2 km) of a point for c) April 29 and d) October 7, based on data from 1982–2011 (SPC 2023b).

Based on data from 1982–2011 for April 29 (SPC 2023b), the probability of ≥2-in (5.1-cm) hail within 25 mi (40.2 km) of a point in Cleveland County is 0.7–0.9% (Fig. 1c), while for October 7, the probability is only 0.025–0.075% (Fig. 1d), which is an order of magnitude less than in April. Hail with diameter ≥3 in (7.6 cm) is relatively rare (Gutierrez and Kumjian 2021) and makes up only 1.1% of all United States 1955–2021 hail reports and 1.47% of all Oklahoma 1955–2021 hail reports (SPC 2023c).

Along with the relative rarity of ≥3-in (7.6-cm) hail reports in general, especially on two dates in a single year for the same location, these two very long-lived (>5 h), 2021 hailstorms were intriguing in that the April storm was situated behind a surface wind-shift boundary, and remained sub-severe until it approached the boundary, while the October storm was off-season (or second season) for significant hail.

To demonstrate the reasons why these two ≥3-in (7.6-cm) hailstorms that affected Norman in 2021 were chosen for investigation, we present case studies that show: 1) that the April storm appeared anomalous in that its environmental parameters were marginal for large hail, and that it exhibited somewhat unusual radar characteristics as a rather small, but long-lasting, hail-producing supercell; thus, it will be given particular emphasis. Furthermore, while situated behind a surface wind-shift boundary, the April storm changed morphology about 30 mi (48.3 km) west of the center of Norman, owing to proximity to the boundary and subtle environmental changes; 2) that the 2021 October storm was the only ≥3-in (7.6-cm) hailstorm to affect Norman (or

Cleveland County) outside of the months of April or May and one of the few ≥3-in (7.6-cm) October hailstorms ever in Oklahoma (≈3% of all ≥3-in or 7.6-cm 1955–2021 Oklahoma hail reports were in the month of October; SPC 2023c); and 3) that compared with the six other ≥3-in (7.6-cm) hailstorm dates in Cleveland County from 1955–2021, both 2021 storms of interest had lower CAPE values and larger deep- shear values. Herein, "shear" means the vertical bulk-wind difference or shear-vector magnitude [e.g., 3–6-km shear means the difference between the wind speed magnitude at 6 km height AGL and the wind speed magnitude at 3 km height AGL, unless stated otherwise.

This finding listed in point 3) above supports the results of Nixon and Allen (2022; hereafter NA22) and others, that for hail-producing supercells (as is the case for tornadic storms, e.g., Brooks et al. 2003), either large shear or large buoyancy are needed for large hail, and that more of one can compensate for lack of the other (e.g., Johns et al. 1993; NA22). This can also be inferred from the results of Johnson and Sugden (2014; hereafter JS14) in that while shear alone or CAPE alone might not show good hail-size discrimination, composite parameters, such as the significant severe parameter [SSP; SSP = product of mixed-layer CAPE (MLCAPE) and 0–6 km wind shear; Craven and Brooks 2004] or the large hail parameter (LHP; JS14), improve that discrimination, which implicitly supports that larger values of one of buoyancy or shear can compensate for lower values of the other.

It is not a goal of this paper to identify the physics and dynamics of hail formation in these two 2021 hailstorms, although hail-favorable characteristics and conditions are noted when observed and discussed in the context of prior studies in the literature.

Data and methodology, and associated limitations of each, are discussed in section 2. Storm reports and observations are described in section 3. Section 4 documents the environmental conditions. Storm evolution, as depicted in radar and polarimetric presentations, are shown in sections 5 and 6, respectively. Section 7 presents a comparison with the other ≥3-in (7.6-cm) Cleveland County hailstorms. A summary and conclusions are provided in section 8.

2. Data and methodology

Severe-storm reports were obtained from Storm Data (NCEI 2023a) and/or the SPC-maintained severe-weather database (https://www.spc.noaa.gov/wcm/; SPC 2023c; severe thunderstorm criteria are hail ≥1 in or 2.54 cm, and/or winds ≥58 mph or 25.9 m s^{-1}, and/or a tornado). Hail swaths (maximum expected size of hail, MESH; Witt et al. 1998a), rotation tracks, and 12-h rainfall maps were generated using MRMS (Multi-Radar Multi-Sensor; Witt et al. 1998a; Smith et al. 2016; Zhang et al. 2016; NSSL 2023). Soundings were obtained from SPC, University of Wyoming (2023), and Iowa State University (2023) sounding archives. Sounding data and calculated parameters from observations and numerical models were generated using the Sounding and Hodograph Analysis and Research Program in Python (SHARPpy; Blumberg et al. 2017) and calculations by the authors (e.g., LHP, JS14; FORTRAN code available from the authors upon request).

Limitations of hail reports from the NCEI Storm Data dataset have been discussed substantially by prior researchers. Examples include biases in reporting related to population density or observer/observational network density (e.g., Schaefer et al. 2004; Doswell et al. 2005; Allen and Tippett 2015). In addition, report sizes are often evaluated using comparisons to common objects, which results in hail-size misidentification, based on the relative-object perceived size and resultant artificial binning of a continuous hail-size spectrum into size categories (Schaefer et al. 2004; Doswell et al. 2005; Allen and Tippett 2015; Blair et al. 2017). There also is a tendency to report the most severe event (Morgan and Summers 1982), such that in the presence of damaging wind or tornadoes, hail reports might be neglected. In support of this, Kelly et al. (1985) report that for 1955–1983, only 4% of tornado reports also had accompanying hail reports, despite that these are often observed to occur together (e.g., Witt et al. 1998b).

Furthermore, with regard to hail-report accuracy, Witt at al. (1998a) found 29% of 115 hail reports on 10 storm days had locations and times that were not well-correlated with WSR-88D radar data, and Blair et al. (2011) found 24% of reports for 1995–2009 did not have consistent radar support. Lastly, the largest observed hail size in studies using finescale

observing networks or hailpads is virtually never the maximum hail size (Morgan and Towery 1975; Bardsley 1990), so that reports are skewed toward less severe sizes. As a result, there may have been more ≥3-in (7.6-cm) cases in central Oklahoma that were not documented, and these events might not be as rare as they appear. Alternatively, maximum hail size with both the April and October 2021 storms may have been larger than the reported sizes.

Changes in hail reporting have also affected the robustness of the dataset. In 1972, SPC and NCDC (now NCEI) began to synchronize their datasets, resulting in incomplete data for the year 1972 (Schaefer et al. 2004). Also, in 2010, the threshold for severe hail was increased from 0.75 in (1.9 cm) to 1 in (2.5 cm), which has been shown to strongly affect statistical studies (Allen and Tippett 2015). Lastly, there has been an increase in hail reports with time without a meteorological basis (Brooks and Dotzek 2008; Allen et al. 2015). Increased reports from social media and storm chasers, and increased cell-phone availability (Allen et al. 2015), could be factors in this trend, which makes the separation of real meteorological increases in hail difficult to distinguish from reporting changes.

Hail reports of ≥3 in (7.6 cm) were examined for Cleveland County (area of 558 mi^2 or 1445.2 km^2) and the Norman, municipal limits (area of 189.42 mi^2 or 490.6 km^2). *Storm Data* (NCEI 2023a) hail reports visually were determined to be within these geographic regions using the latitude and longitude for each hail report, and comparing the locations with the plotted geographic region boundaries in Datawrapper software and in Google Maps.

Some radar-derived values and features were subjectively and visually obtained from data displayed by the Weather and Climate Toolkit (WCT; NCEI 2023b) radar-viewing software graphics and MRMS graphics, which may have impacted precision and accuracy.

Additionally, like most hail-size estimation techniques that use reflectivity, MESH can underestimate hail size (Bunkers and Smith 2013; Ortega 2018). Specifically, because MESH is related to a weighted vertical integral of reflectivity between the freezing level and –20°C height, underestimation is more common in highly tilted storms embedded in strong deep-layer shear, supercells that possess a large bounded weak echo region (BWER), left-moving supercells, and/or storms with low-density, dry hailstones (e.g., Straka et al. 2000). The dependence of MESH on other factors besides hail size, including changes between dry hail and wet hail, the presence of very large raindrops, changes in microphysical particle shapes, and their fall characteristics, should be kept in mind when interpreting the MESH values presented.

Another limitation was the absence of an observed 0000 UTC sounding from Norman (KOUN) on 29 April 2021 (although there was a KOUN 1800 UTC special sounding on 28 April 2021). A model-derived, High-Resolution Rapid Refresh (HRRR; 3-km horizontal resolution and 1-h temporal output resolution; Dowell et al. 2022) sounding at the KOUN location at 0100 UTC 29 April 2021 F000 (forecast hour zero) was used instead as a proximity sounding for this case.

3. Storm reports

The April storm affected Norman starting at about 0150 UTC on 29 April 2021 and caused extensive damage. The storm report stated (NCEI 2023c):

"Storms continued into the 28th as a slow-moving trough approached. Early morning convection produced numerous flood reports. Later in the day, renewed storm development led to an isolated supercell which tracked across southern portions of the OKC metro area with 2–3 diameter hail and damaging winds. Extensive damage was reported with this storm, with the most significant damage concentrated in Norman. In Cleveland County, the hail and wind caused over 2 million dollars in damage just to county-owned buildings. While exact numbers for private homes, businesses and vehicles are not available, damage estimates are easily into the hundreds of millions of dollars."

The October storm affected Norman at about 0050 UTC 11 October 2021, about 1 h earlier than the April storm. The October storm occurred with a surface cold front, in an environment with larger buoyancy than the April storm, had a history of tornadoes, and occurred along with several other storms in Oklahoma. Storm reports included the following narrative (NCEI 2023d):

"An unseasonably warm and moist airmass was in place across the region ahead of a powerful upper wave moving out of the 4 corners region. This led to the development of numerous

severe thunderstorms across Oklahoma and Texas during the afternoon and evening of the 10th. Several tornadoes were reported, along with hail larger than baseballs that impacted Norman, OK for the second time in six months, leading to millions of dollars in damages once again to homes, cars, and businesses."

Examples of the damage and the hailstones from both 2021 storms of interest are shown in Fig. 2. In particular, photos from west Norman associated with the April storm show window damage (Fig. 2a) and hailstones (Fig. 2b). The stone with the largest axis length (bottom left), estimated using the coin size from the photo to have been ≈3.1 in (7.8 cm), had prominent protuberances. Additional photos show the damage associated with the October storm from central Norman (Fig. 2c) and hailstones (Fig. 2d) from western Norman, where the largest (bottom) is estimated visually using the coin size from the photo to have been ≈2.8 in (7.1 cm).

Oklahoma hail and tornado reports and selected wind reports for 28–29 April 2021 and 10–11 October 2021 are shown in Table 1. All 1955–2021, ≥3-in (7.6-cm) and 2.75-in (7-cm) ≤ d <3-in (7.6-cm) Norman hail report locations are shown in Fig. 3. The largest Norman hailstone associated with the April storm was reported at 2012 UTC (Table 1), with a measured 3.2-in (8.1-cm) size, which was the second largest hail size report for Norman, next to the 3.25-in (8.3-cm) hailstone reported on 4 May 2020 (Fig. 3a). The largest reported hail size associated with the October storm in Norman was 3 in (7.6 cm; Fig. 3a; Table 1). To put these two 2021 ≥3-in (7.6-cm) hailstorms into historical perspective, from 1955–2021, in Norman, there have been only seven ≥3-in (7.6-cm) hail reports on five different dates (Fig. 3a), of which three reports occurred with the 2021 hailstorms. Furthermore, there were only eight 2.75–2.99-in (7–7.6-cm) hail reports (Fig. 3b) from 1955–2021 in Norman on four different dates. Of these eight reports, five occurred with the April storm and one with the October storm (i.e., six of the eight occurred with the two 2021 storms of interest). None of the 3-in (7.6-cm), 1955–2021 Norman reports occurred outside of the months of April–May, except the 10–11 October 2021 report.

Based on these hail reports, ≥2.75-in (7-cm) hail in Norman is certainly infrequent, which makes the two 2021 events rather exceptional. Moreover, the likelihood of two ≥3-in (7.6-cm) hailstorms striking twice in one year within the 189.42 mi^2 (490.6 km^2) area of the city limits of Norman is extremely small. Granted, this is a small area relative to the area of a circle with radius 25 mi (40.2 km), which is 1963.5 mi^2 (5085 km^2), as used for Fig. 1 probabilities.

4. Environmental conditions

a. Synoptic

On 0000 UTC 29 April 2021, a 300-hPa longwave trough and its southwesterly jet (maximum wind speeds 100–120 kt (51.4–61.7 m s^{-1}) remained west of the storm region (Fig. 4a). An accompanying extensive northeast-southwest oriented, positively tilted 500-hPa (Fig. 4b) large-scale, upper-air trough axis at 0000 UTC was in place from eastern Colorado to western New Mexico, with a cutoff low in southwestern New Mexico. The upper and mid-level system were accompanied by strong 50–65 kt (25.7–33.4 m s^{-1}) 500-hPa flow, and 75–100 kt (38.6–51.4 m s^{-1}) 300-hPa flow over south-central Texas through central Oklahoma, that provided substantial deep-layer shear.

Table 1 *(next page)*: NCEI hail, selected wind (light grey), and tornado (in dark grey) reports associated with the 28–29 April 2021 (top) and the 10–11 October 2021 (bottom) storms, prior to, and just after each storm affected Norman. Column two contains either hail size (in) for a hail report, wind speed (sp; kt) for a wind report, or a tornado report (TORN). Column three contains hail size (cm), wind speed (m s^{-1}) or EF rating. *Based on radar, this 2-in (5.1-cm) hail at the Roosevelt, OK location at 2315 UTC on 10 October, likely occurred around 2300 UTC. †These reports were not in the NCEI storm events database, but were included in the SPC interactive preliminary local storm reports (LSR; SPC 2023d) and were measured by Oklahoma Mesonet, and thus, they are included here, with the caveat that they are not in the official NCEI records. Oklahoma counties that appear in these reports (except for Jackson County in extreme southwest Oklahoma), are shown in red font in Fig. 6a.

28 APR Time (UTC)	Size (in) Sp (kt) Tornado	Size (cm) Sp (m s^{-1}) F/EF	Location	County	Latitude	Longitude
0134	1.75	4.4	BRIDGE CREEK	GRADY	35.23	–97.72
0134	52	26.8	BRIDGE CREEK	GRADY	35.23	–97.72
0138	65	33.4	3 SW BRIDGE CREEK	GRADY	35.2	–97.76
0138	1.75	4.4	3 SW BRIDGE CREEK	GRADY	35.2	–97.76
0138	2.75	7.0	2 SSE BRIDGE CREEK	GRADY	35.2	–97.71
0143	1.75	4.4	3 WNW NEWCASTLE	MCCLAIN	35.26	–97.65
0144	2.75	7.0	2 NNE BLANCHARD	MCCLAIN	35.16	–97.64
0145	1.75	4.4	1 WSW NEWCASTLE	MCCLAIN	35.24	–97.62
0145	61	31.4	1 WSW NEWCASTLE	MCCLAIN	35.24	–97.62
0153	2.75	7.0	4 NW NORMAN	CLEVELAND	35.26	–97.49
0153	2.75	7.0	4 W NORMAN	CLEVELAND	35.22	–97.51
0154	1.25	3.2	5 S MOORE	CLEVELAND	35.27	–97.5
0154	1.75	4.4	5 NW NORMAN	CLEVELAND	35.27	–97.5
0155	1.50	3.8	4 NW NORMAN	CLEVELAND	35.26	–97.5
0155	2.75	7.0	3 WNW NORMAN	CLEVELAND	35.23	–97.49
0157	2.75	7.0	2 WNW NORMAN	CLEVELAND	35.23	–97.47
0157	3.00	7.6	1 NW NORMAN	CLEVELAND	35.23	–97.45
0158	1.75	4.4	3 NNW NORMAN	CLEVELAND	35.26	–97.46
0159	2.50	6.4	4 W NORMAN	CLEVELAND	35.22	–97.51
0200	60	30.9	1 S WESTHEIMER OUN	CLEVELAND	35.24	–97.47
0200	60	30.9	2 NW NORMAN	CLEVELAND	35.24	–97.47
0200	2.75	7.0	2 NNE NORMAN	CLEVELAND	35.25	–97.42
0212	3.00 M3.2	7.6 M8.1	6 W LAKE THUNDERBIRD	CLEVELAND	35.22	–97.34
0238	1.00	2.5	3 NW BETHEL ACRES	CLEVELAND	35.33	–97.09
0322	1.75	4.4	CENTERVIEW	POTTAWATOMIE	35.43	–96.67
10 OCT Time (UTC)	**Size (in) Sp (kt) Tornado**	**Size (cm) Sp (m s^{-1}) F/EF**	**Location**	**County**	**Latitude**	**Longitude**
2216	1.25	3.2	3 NW ELMER	JACKSON	34.51	–99.39
2227	1.00	2.5	ALTUS AIR FORCE BASE	JACKSON	34.66	–99.29
*2315	2.00	5.1	ROOSEVELT	KIOWA	34.85	–99.02
2259	TORN	EFU	4 SSW COOPERTON	KIOWA	34.82	–98.90
2313	TORN	EF1	8 E COOPERTON	KIOWA	34.89	–98.73
2320	TORN	EF1	9 W BOONE	CADDO	34.9	–98.62
2345	TORN	EF2	2 SW ANADARKO	CADDO	35.04	–98.30
†0000	62	31.9	4 ENE APACHE	CADDO	34.92	–98.29
0002	TORN	EFU	5 S LAKE CHICKASHA	CADDO	35.06	–98.11
0004	TORN	EFU	1 S VERDEN	GRADY	35.06	–98.09
†0015	58	29.8	2 SSE CHICKASHA	GRADY	35.01	–97.94
0016	TORN	EFU	3 NE CHICKASHA	GRADY	35.11	–97.93
0040	1.50	3.8	2 WNW DIBBLE	MCCLAIN	35.04	–97.65
0040	1.75	4.4	4 NE BLANCHARD	MCCLAIN	35.19	–97.61
0048	1.00	2.5	NEWCASTLE	MCCLAIN	35.25	–97.6
0051	1.00	2.5	GOLDSBY	MCCLAIN	35.15	–97.48
0057	1.75	4.4	3 SE GOLDSBY	MCCLAIN	35.12	–97.44
0057	1.00	2.5	1 NNE NOBLE	CLEVELAND	35.15	–97.39
0102	1.50	3.8	2 E NOBLE	CLEVELAND	35.14	–97.36
0104	3.00	7.6	2 E NORMAN	CLEVELAND	35.22	–97.41
0105	2.00	5.1	2 NW NORMAN	CLEVELAND	35.24	–97.46
0106	2.75	7.0	5 NE NORMAN	CLEVELAND	35.26	–97.37

Figure 2: a) Window damage from the 28–29 April 2021 storm from west Norman (credit: Alison Petrone). b) Hailstones from the April storm from west Norman (credit: Denea Sadler). Using the diameter of the half-dollar coin (diameter = 30.6 mm; left coin in photo), the hailstone nearest the half-dollar was visually estimated to have had a long axis of about 3.1 in (78 mm). c) Window damage from the 10–11 October 2021 storm in central Norman (credit: Zach Rael). d) Hailstones from the October storm from west Norman (credit: Tonya Faires). Using the quarter-dollar coin (diameter = 24.3 mm), the longest axis of the larger hailstone in the bottom of the photo was visually estimated at about 2.8 in (71 mm).

A prominent 500-hPa shortwave trough from north-central Texas to the northern Texas Panhandle, and a weaker 500-hPa shortwave trough near the Rio Grande Valley along the Texas-Mexico border, provided synoptic-scale lift to aid in the convective environment in Oklahoma and Texas.

Also at 0000 UTC 29 April 2021, a 700-hPa moisture axis (Fig 4c) was situated ahead of a trough axis and analyzed stationary front at the surface (Fig. 4d; moisture axis also identifiable at 850 hPa, not shown). The front separated drier air to the west from moister air to the east, and extended from western Texas, north to western Oklahoma and northeast to west-central Missouri. Low-level convergence ahead of the surface front helped provide lift to support storm initiation and maintenance, especially northward of a surface low southwest of the Rio Grande, from south central to north central Texas, to a very weak (1006-hPa) surface low in southern Oklahoma (along the Red River), and then northeastward to west-central Missouri.

Many aspects of the synoptic pattern were similar on 10–11 October 2021. The southern portion of a positively tilted 300-hPa trough moved from about the four corners region at 1200 UTC to west Texas at 0000 UTC (Fig. 4e), remaining west of the storm area in Oklahoma and Texas. Also at 0000 UTC, a 300-hPa jet maximum of over 115 kt (59.2 m s^{-1}) was situated over central and western Oklahoma, extending into north and west Texas. Meanwhile, a 500-hPa cutoff low was evident over the Texas Panhandle, with a near-meridional trough extending southward (Fig. 4f).

A shortwave trough also was evident farther east, from northwestern to southeastern Oklahoma. Winds at 500 hPa were >60 kt (30.9 m s^{-1}), with difluent flow over central Oklahoma. A tight moisture gradient at 700 hPa (Fig. 4g) existed above the surface front (Fig. 4h), separating a deep moist air mass from drier air to the west, while a cold front was analyzed to the northeast and southwest of a 994-hPa surface low near the Red River.

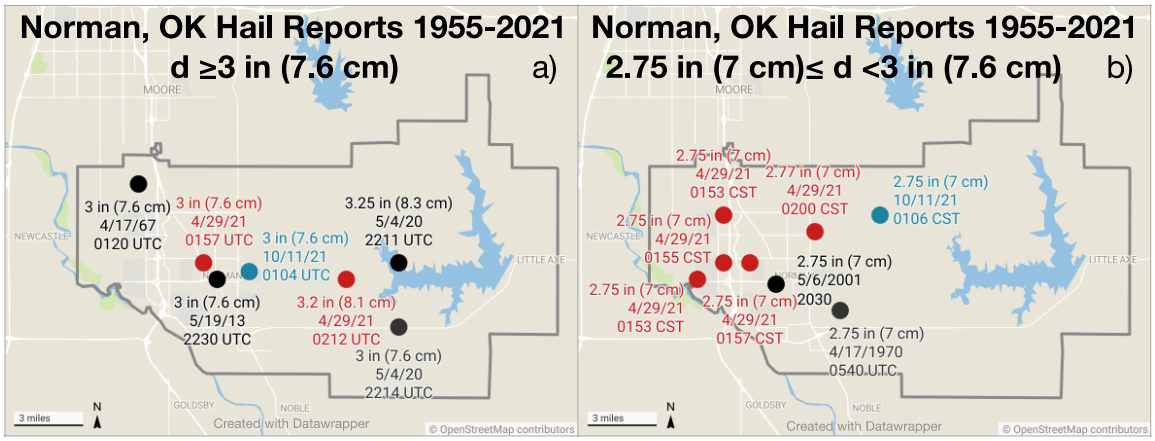

Figure 3: Norman, OK (light grey outline) hail reports from NCEI for 1955–2021: a) diameter, d ≥3 in (7.6 cm) and b) 2.75 in (7.0 cm) ≤d <3 in (7.6 cm). Reports from 28–29 April 2021 are in red, from 10–11 October 2021 in blue, and reports from other years are in black. The latitude and longitude of a 3-in (7.6-cm) hail report from 19 May 2013 were coincident with the center of Norman (and are plotted as such); however, the NCEI event narrative states the location at "12th and Tecumseh," while SPC-maintained reports state "E. 12th and Tecumseh." In addition, for a 3-in (7.6-cm) hail report on 17 April 1967, the latitude and longitude were within Norman, but the location was given as Moore, OK. Thus, whether or not this hailstone was in Norman, or to the north in Moore, is uncertain. The latitude and longitude are taken to be correct herein and so this case was included. The latitude and longitude for a 2.75-in (7-cm) hail report on 06 May 2001 were different in NCEI than in the SPC-maintained reports (NCEI location was plotted and both locations were within Norman). From 1 January 2022 to 31 December 2022 there were no other ≥2.75-in (7-cm) hail reports in Norman.

In summary, both dates were characterized by positively tilted upper-level troughs across the Mountain West, with mid-level shortwave troughs across the Red River/North Texas for 0000 UTC 29 April 2021, and across Oklahoma for 0000 UTC 11 October 2021. Over Oklahoma, the 300-hPa maximum wind was slightly larger in October, but the region of ≥100-kt (51.4-m s^{-1}) winds was much broader in April. Both dates also had surface lows near the Red River.

b. Upper-air soundings

Severe-hail forecasts can be aided by examination of CAPE, mixing ratio of the most-unstable parcel, 700–500-hPa lapse rate, 500-hPa temperature, and 0–6-km bulk shear, which are combined in the significant hail parameter (SHIP; SPC 2023f) developed by SPC to aid in the delineation of significant (≥2-in or 5.1-cm) and nonsignificant (<2-in or 5.1-cm) hail. It is not a hail-size forecast parameter, but rather is intended for diagnostic purposes (Doswell and Schultz 2006).

In addition, the large hail parameter (LHP), developed by Johnson and Sugden (2014), was designed to distinguish hail with diameter ≥3.5 in (8.9 cm) from hail with diameter <2 in (5.1 cm). They state, "The LHP formula creates improved skill by including non-traditional environmental parameters typically associated with storm longevity, precipitation efficiency, and hail-growth rates." In particular, variables included in the LHP that are not included in SHIP or the SSP are the –10°C to –30°C layer thickness (hail-growth-zone thickness, THK_{HGZ}, e.g., Nelson 1983), and wind-related variables, including various layer directional differences and 0–EL (equilibrium level) shear (Appendix A). The LHP is also a diagnostic and not a prognostic hail parameter.

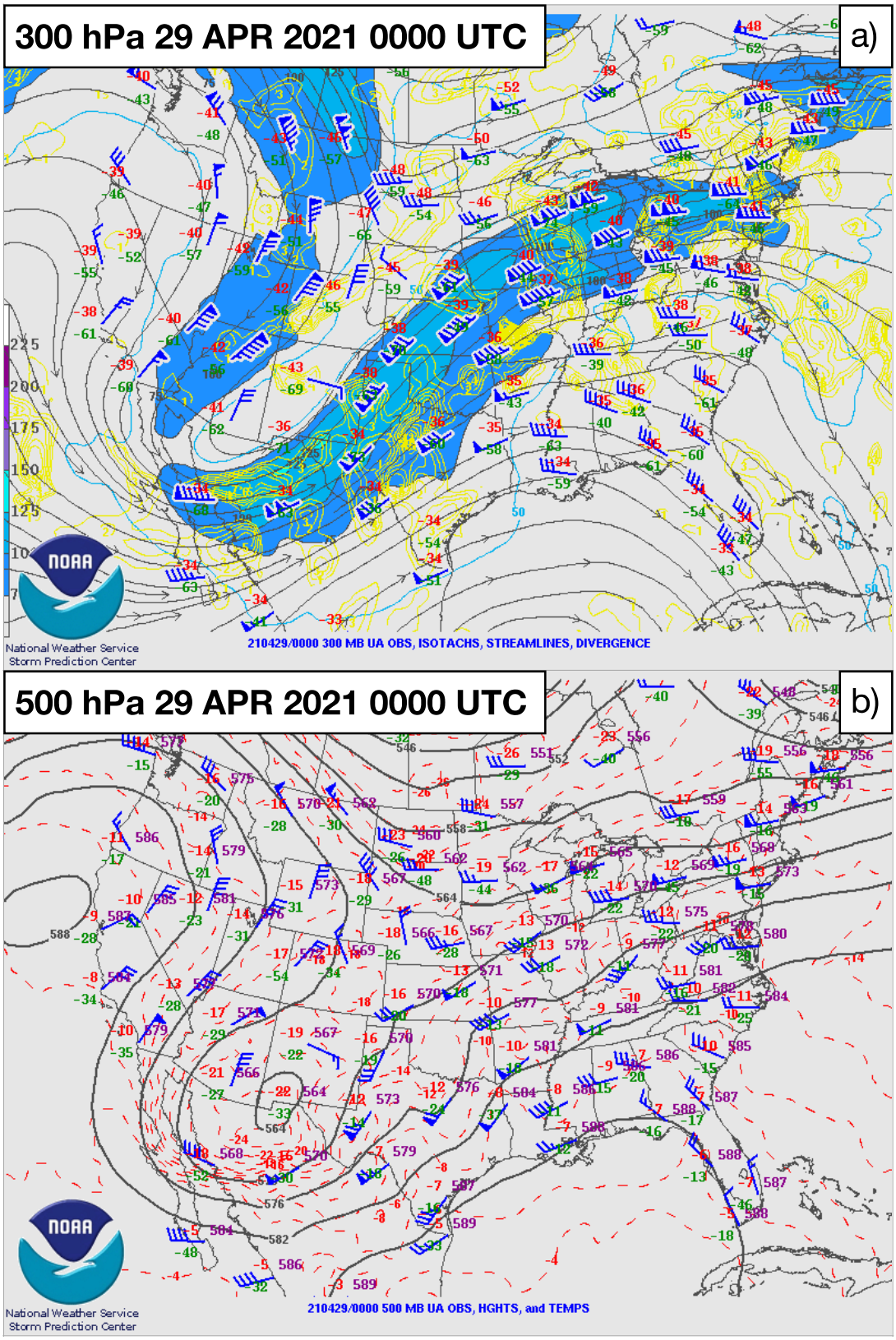

Figure 4 *(Next 4 pages).*

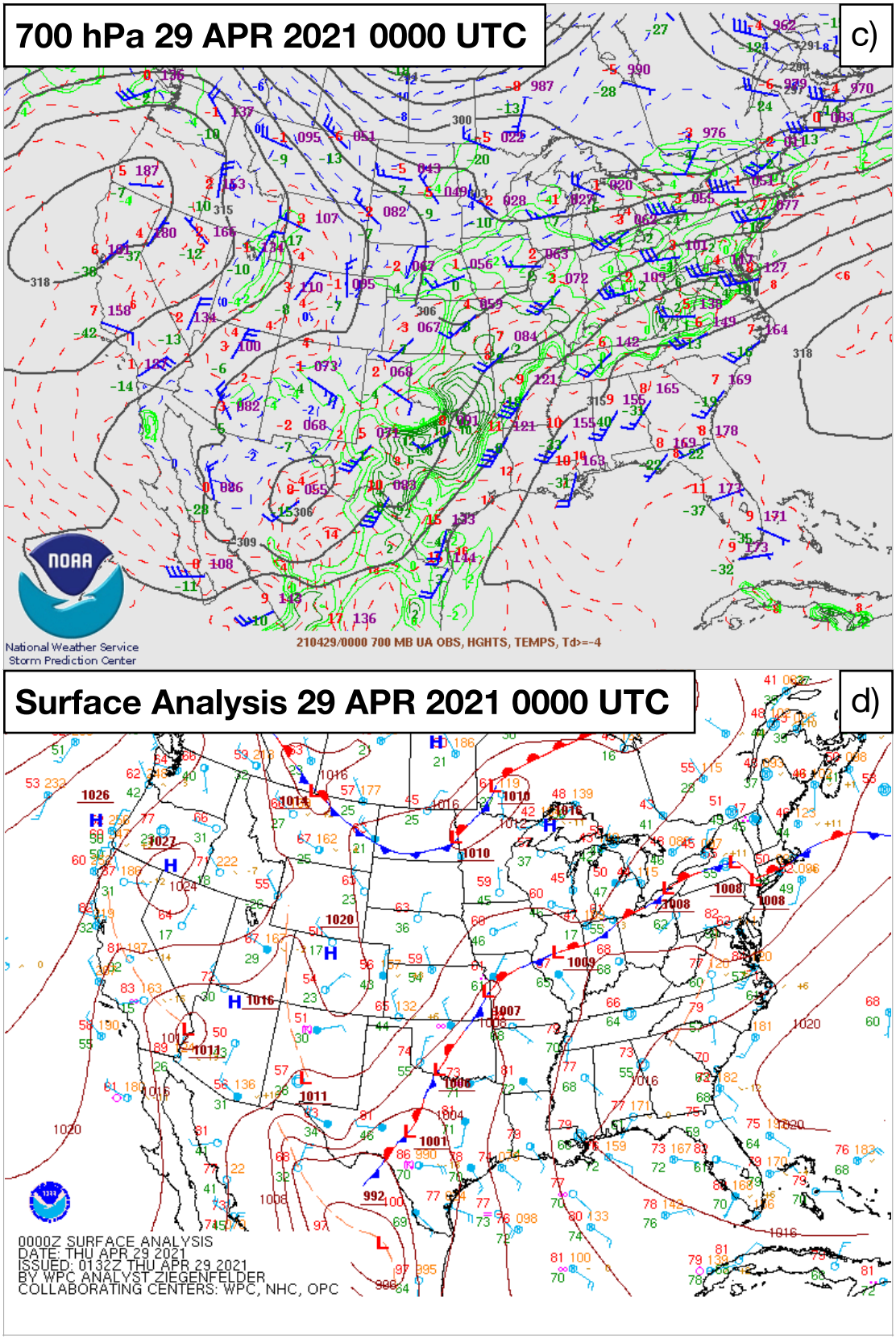

Figure 4 *continued.*

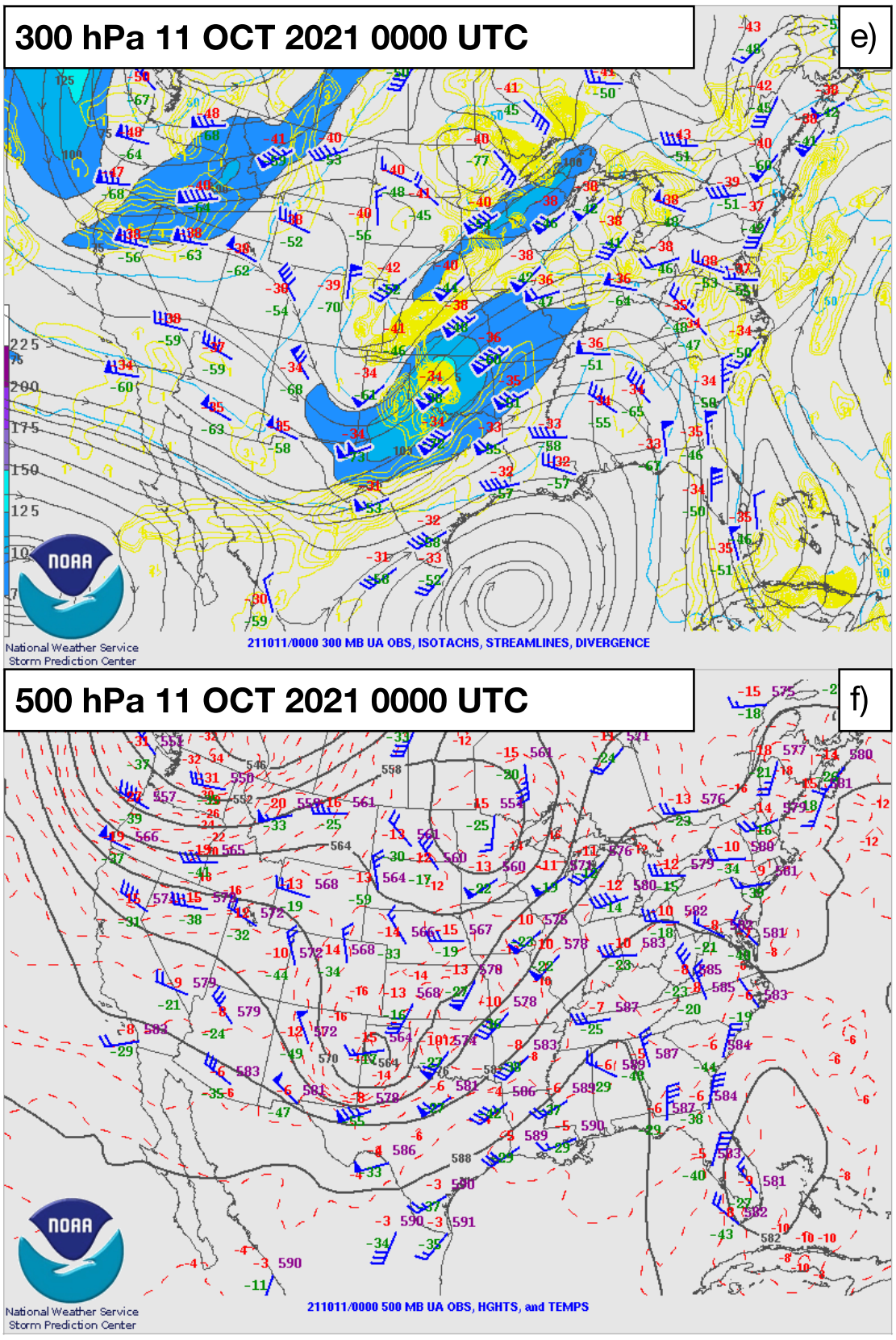

Figure 4 *continued.*

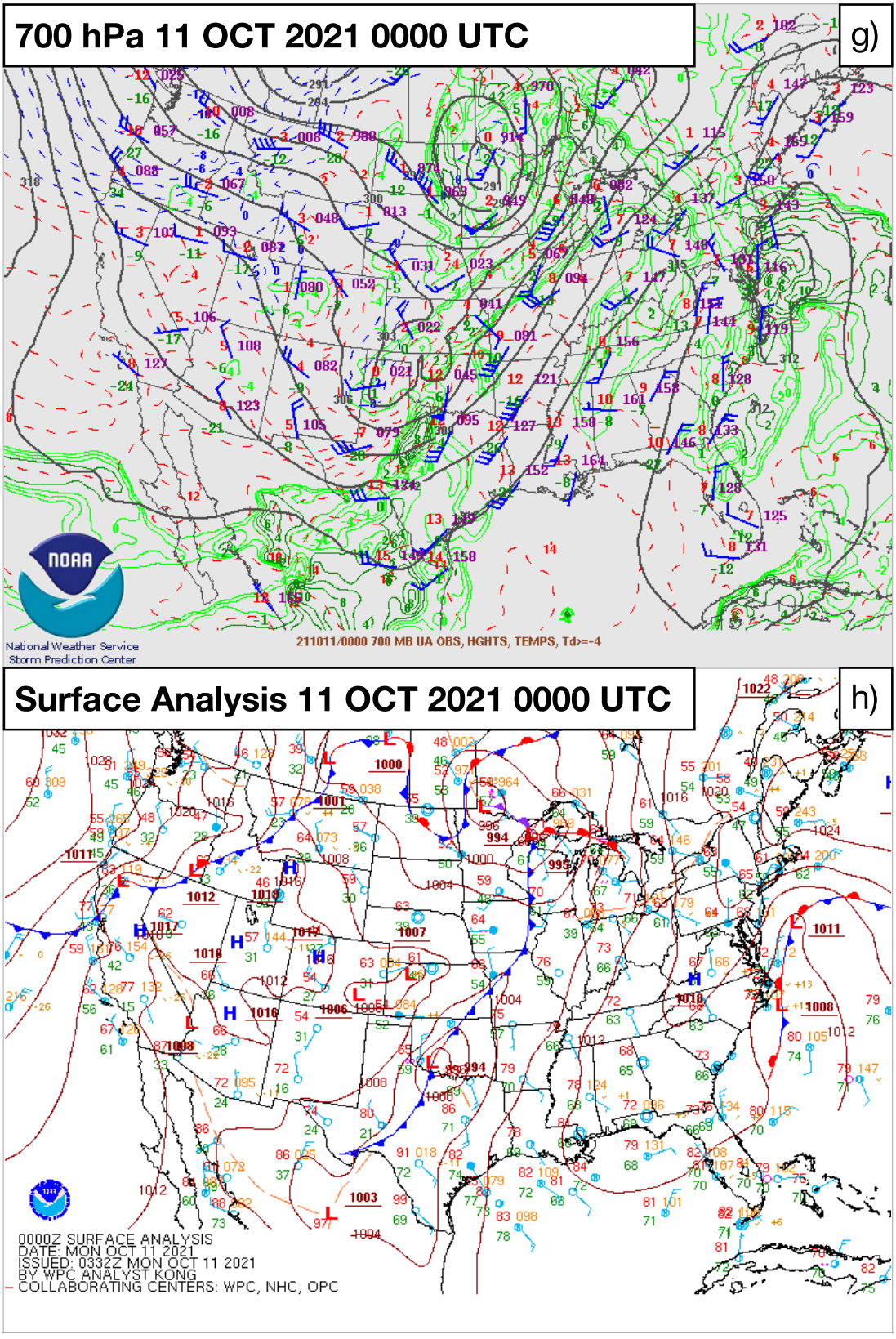

Figure 4: Upper-air charts and surface analyses at 0000 UTC 29 April 2021 (a–d) and 0000 UTC 11 October 2021 (e–h). a) and e) 300-hPa isotachs in (blue; 25-kt contour interval), streamlines (black), and

divergence (yellow). Conventional station plot with temperature (red), dewpoint temperature (green; ˚C), and winds (pennant = 50 kt or 25.7 m s^{-1}; full barb = 10 kt or 5.1 m s^{-1}; half-barb = 5 kt or 2.6 m s^{-1}). b) and f) 500-hPa geopotential heights (black; 60-m contour interval); isotherms (red dashed; ˚C; 2˚C contour interval). Conventional station plot as in a) and e). c) and g) As in b) and f), but for 700-hPa geopotential heights (black; dam; 30-m contour interval; isotherms (red dashed; 2˚C contour interval) and isodrosotherms ≥–4˚C (green; 2˚C contour interval). Conventional station plot as in a) and e). d) and h) Weather Prediction Center (WPC) surface analyses. MSL pressure (brown; 4-hPa contour interval). Conventional station plot with temperature (red; ˚F), dewpoint temperature (green; ˚F), and winds (pennant = 50 kt or 25.7 m s^{-1}; full barb = 10 kt or 5.1 m s^{-1}; half-barb = 5 kt or 2.6 m s^{-1}; concentric circles = calm). Maps from SPC (2023e).

At Norman, a regular NWS observed 0000 UTC 29 April 2021 sounding was not available, although if it were, it would have been a reasonably good proximity sounding in time and space (e.g., Jewell and Brimelow 2009, 100 n mi or 185 km and 2.5 h from 2330 UTC; Thompson et al. 2003; Craven and Brooks 2004) for the April storm. Instead, the KOUN 29 April 2021 0100 UTC HRRR F000 (forecast hour zero) sounding was selected to represent the approximate environment of ahead of the passage the April storm through Norman, and is used for all discussion herein of that environment.

Comparison of the soundings selected to represent proximity soundings at 0100 UTC 29 April 2021 and at 0000 UTC 11 October 2021 (Fig. 5; last two columns of Table 2, shown later in section 7) shows that the most-unstable parcel (MU)CAPE, for the April and October dates, was 1306 J kg^{-1} and 1932 J kg^{-1}, respectively. The April MUCAPE falls near or just below the 10th percentile in the distribution for nonsupercell storms shown by Blair et al. (2017, their Fig. 11a), while the October MUCAPE satisfies their threshold for marginal supercells (≥1832 J kg^{-1}). Furthermore, the MUCAPE for the April storm does not meet the threshold value of JS14 for ≥2-in (5.1-cm) hail, MUCAPE ≥1850 J kg^{-1}, while the October value does. However, MUCAPE values <1909 J kg^{-1} do exist for ≈25% of the cases for 2–3.25-in (5.1–8.3-cm) hail (JS14, their Fig. 8), such that the October (April) MUCAPE value of 1932 (1306) J kg^{-1} falls just above 25% (≈15%) in the distribution. Statistically, the April and October MUCAPE values do not exclude the possibility of significant hail.

In contrast, the 0–6-km shear-vector magnitudes of 67 kt (34.5 m s^{-1}) and 71 kt (36.5 m s^{-1}) for the April and October storms, respectively, exceeded the ≥2-in (5.1-cm) hail threshold of 38.9 kt (20 m s^{-1}; JS14). The larger values for even deeper shear, 0–EL magnitudes of 95.2 kt (49 m s^{-1}) and 89.4 kt (46 m s^{-1}) for the April and October dates, respectively, were strongly favorable for hail growth (JS14's ≥2-in or 5.1-cm hail 0–EL shear threshold was 46.7 kt or 24 m s^{-1}; see also Dennis and Kumjian 2017). Additionally, the 0–8-km shear-vector magnitudes, 76 and 108 kt (39.1 and 55.6 m s^{-1}), for April and October, respectively, would support long-lived supercells based on prior studies (e.g., Bunkers et al. 2006 a,b; Davenport 2021). Specifically, Bunkers et al. (2006b, their Fig. 1) showed that long-lived (≥4 h) supercells were more likely with 0–8-km shear-vector magnitudes greater than ≈62 kt (32 m s^{-1}).

For the April model sounding, the 0–1-km, 0–3-km, and effective storm-relative helicity (SRH and EffSRH; Thompson et al. 2007) were –47, 78 and 22 m^2 s^{-2}, respectively. The 0–1-km and 0–3-km shear-vector magnitudes (12 and 16 kt or 6.2 and 8.2 m s^{-1}, respectively) did not strongly indicate cyclonic supercells (e.g., Rasmussen and Blanchard 1998; Rasmussen 2003), although the upper-level winds were sufficiently strong (see also Fig. 4a). In contrast, low-level hodograph curvature for the October date (Fig. 5b) was associated with much larger values of 0–1-km, 0–3-km SRH and EffSRH (183, 255, and 246 m^2 s^{-2}) and larger 0–1-km and 0–3-km shear-vector magnitudes (20 and 41 kt or 10.3 and 21.1 m s^{-1}) than those of the April date and thus appear more consistent with cyclonic, and in this case, tornadic supercells, which were observed.

These two 2021 hailstorm environmental characteristics support the conclusions of Lin and Kumjian (2022) and references therein, that CAPE alone is not a good hail-size discriminator (i.e., larger CAPE does not always correspond to larger hail sizes) and that horizontal winds, updraft area, and storm morphology possibly are most important to hail-growth residence times. Edwards and Thompson (1998) also showed that CAPE was not a good hail-size discriminator

A

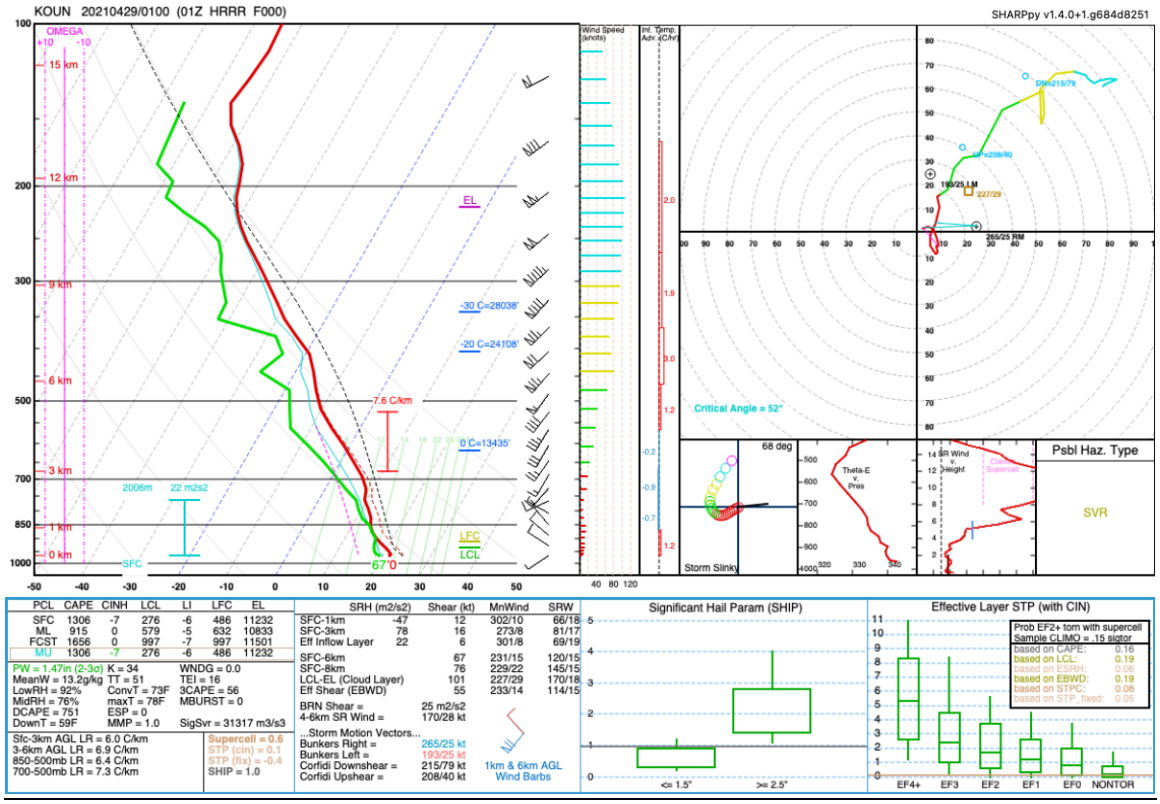

PCL	CAPE	CINH	LCL	LI	LFC	EL
SFC	1306	-7	276	-6	486	11232
ML	915	0	579	-5	632	10833
FCST	1656	0	997	-7	997	11501
MU	1306	-7	276	-6	486	11232

PW = 1.47in (2-3cl)	K = 34		WNDG = 0.0
MeanW = 13.2g/kg	TT = 51		TEI = 16
LowRH = 92%	ConvT = 73F		3CAPE = 56
MidRH = 76%	maxT = 78F		MBURST = 0
DCAPE = 751	ESP = 0		
DownT = 59F	MMP = 1.0		SigSvr = 31317 m3/s3

Sfc-3km AGL LR = 6.0 C/km	Supercell = 0.6
3-6km AGL LR = 6.9 C/km	STP (cin) = 0.1
850-500mb LR = 6.4 C/km	STP (fix) = -0.4
700-500mb LR = 7.3 C/km	SHIP = 1.0

	SRH (m2/s2)	Shear (kt)	MnWind	SRW
SFC-1km	-47	12	302/10	66/18
SFC-3km	78	16	273/8	81/17
Eff Inflow Layer	22	6	301/8	69/19
SFC-6km		67	231/15	120/15
SFC-8km		76	229/22	145/15
LCL-EL (Cloud Layer)		101	227/29	170/18
Eff Shear (EBWD)		55	233/14	114/15

BRN Shear =	25 m2/s2
4-6km SR Wind =	170/28 kt
...Storm Motion Vectors...	
Bunkers Right =	265/25 kt
Bunkers Left =	193/25 kt
Corfidi Downshear =	215/79 kt
Corfidi Upshear =	208/40 kt

1km & 6km AGL Wind Barbs

B

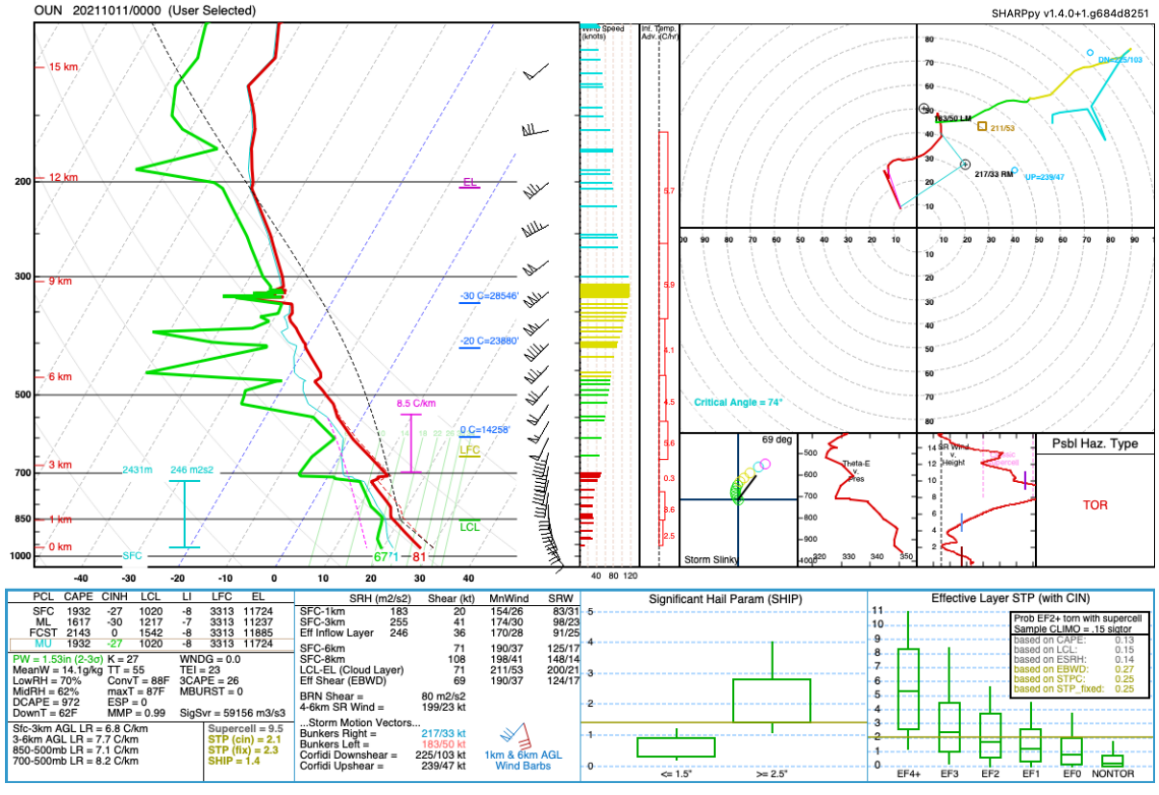

PCL	CAPE	CINH	LCL	LI	LFC	EL
SFC	1932	-27	1020	-8	3313	11724
ML	1617	-30	1217	-7	3313	11237
FCST	2143	0	1542	-8	3313	11885
MU	1932	-27	1020	-8	3313	11724

PW = 1.53in (2-3cl)	K = 27		WNDG = 0.0
MeanW = 14.1g/kg	TT = 55		TEI = 23
LowRH = 70%	ConvT = 88F		3CAPE = 26
MidRH = 62%	maxT = 87F		MBURST = 0
DCAPE = 972	ESP = 0		
DownT = 62F	MMP = 0.99		SigSvr = 59156 m3/s3

Sfc-3km AGL LR = 6.8 C/km	Supercell = 9.5
3-6km AGL LR = 7.7 C/km	STP (cin) = 2.1
850-500mb LR = 7.1 C/km	STP (fix) = 2.3
700-500mb LR = 8.2 C/km	SHIP = 1.4

	SRH (m2/s2)	Shear (kt)	MnWind	SRW
SFC-1km	183	20	154/26	83/31
SFC-3km	255	41	174/30	98/23
Eff Inflow Layer	246	36	170/28	91/25
SFC-6km		71	190/37	125/17
SFC-8km		108	198/41	148/14
LCL-EL (Cloud Layer)		71	211/53	200/21
Eff Shear (EBWD)		69	190/37	124/17

BRN Shear =	80 m2/s2
4-6km SR Wind =	199/23 kt
...Storm Motion Vectors...	
Bunkers Right =	217/33 kt
Bunkers Left =	183/50 kt
Corfidi Downshear =	225/103 kt
Corfidi Upshear =	239/47 kt

1km & 6km AGL Wind Barbs

Figure 5 *(previous page)*: Skew *T*–log*p* diagrams (˚C; hPa) and hodograph (kt) plots from KOUN (Norman, OK) for a) 29 April 2021 0100 UTC HRRR F000 (forecast hour zero) sounding and b) 0000 UTC 11 October 2021, observed. Wind speed and direction given by conventional wind barbs as in Fig. 4. Plots and calculated values produced by SHARPpy for both dates. A moist adiabat associated with the most unstable parcel (the parcel with the maximum equivalent potential temperature value in the lowest 400 hPa) with virtual temperature correction (Doswell and Rasmussen 1994) is indicated in dashed lines. "Storm slinkies" are below the hodographs, where the angle in degrees to the upper right of the slinky is a measure of the updraft tilt. Plots of equivalent potential temperature versus pressure, storm-relative wind versus height and possible hazard type are one, two, and three panels to the right of the slinky, respectively. Bottom right two panel show the significant hail parameter (SHIP) and effective layer significant tornado parameter (STP) distributions. *Click images to enlarge.*

(although they did state no hail with diameter ≥2.75 in or 7.0 cm occurred with CAPE <1300 J kg^{-1}). Additionally, Gutierrez and Kumjian (2021) note a slight association with larger MUCAPE and gargantuan hail (≥6 in or 15.2 cm), and JS14 showed a slight increase in hail size with MUCAPE and MLCAPE, with much overlap. In summary, both the April and October storms had low or moderate values of MUCAPE for significant hail, but values of deep wind shear favorable for ≥2-in (5.1-cm) hail (JS14).

The April sounding LHP was 2.9, which falls below JS14's 25th percentile (LHP = 3.9) for hail of diameter 2–3.25 in (5.1–8.3 cm; JS14, their Fig. 14), while the SHIP value for the April storm was 1.0, which corresponds to just under the 10th percentile (SHIP = 1.1) for hail with diameter ≥2.5 in (6.4 cm). Thus, neither the LHP or SHIP values were more typical values for hail of ≥2-in (5.1-cm) or ≥2.5-in (6.4-cm) diameter, respectively, for the HRRR-derived KOUN 29 April 2021 0100 UTC F000 (forecast hour zero) sounding. However, these lower values do not completely exclude potential for hail of this size since the distributions of LHP and SHIP for ≥2-in (5.1-cm) or ≥2.5-in (6.4-cm) hail, respectively, contain some events with similar values to those for the April date.

In contrast, the October sounding LHP was 16.9, which falls above JS14's 75th percentile (LHP = 13.6) for 2–3.25-in (5.1–8.3-cm) hail, while the SHIP value was 1.4, which falls at the 25th percentile for hail with diameter ≥2.5 in (6.4 cm). Thus, for the October storm, while SHIP performed satisfactorily, the LHP more strongly indicated the potential for hail ≥2 in (5.1 cm). One possible reason for this was that MUCAPE was 1932 J kg^{-1}, but 0–EL km shear was especially large (89.4 kt or 46 m s^{-1}). Therefore, the inclusion of 0–EL wind-related terms increased the value of the LHP, whereas SHIP has four buoyancy-related components and only one wind-related term: 0-6 km shear. Note the buoyant term, the 700–500-hPa lapse rate, was also large at 8.3˚C km^{-1} for the October storm, which is included in both SHIP and LHP.

The SSP performed fairly well for these two storms of interest. The SSP for the April date was 31 317 m^3 s^{-3}, which satisfied the ≥2-in (5.1-cm) hail threshold of JS14 (30 000 m^3 s^{-3}) and Craven and Brooks' (2004) threshold (20 000 m^3 s^{-3}) for significant hail or significant wind (significant wind = gusts ≥65 kt or 33.4 m s^{-1}). In contrast, the October date had an SSP = 59 156 m^3 s^{-3}, which falls within 50–75th percentile for hail of 2–3.25 in (5.1–8.3 cm; JS14, their Fig. 13) and well above the 75th percentile for significant hail or significant wind presented by Craven and Brooks (2004, their Fig. 13; estimate ≈34 000 m^3 s^{-3}). Moreover, the supercell composite parameter (SCP; Thompson et al. 2007) was 0.6 and 9.5 for the April and October dates, respectively, which placed the October storm firmly in the supercell convective mode (Blair et al. 2017, their Fig. 11c), but resulted in the April date having a value entirely below the distribution, even for a nonsupercell.

The hodographs for both the April and October dates (Fig. 5) were quite long and straight, indicating substantial shear, consistent with the association of longer hodographs with large hail (JS14, their Fig. 2; Kumjian and Lombardo 2020; Kumjian et al. 2021, who showed hodographs with larger wind magnitudes above 8 km were associated with larger hail sizes; see also NA22). The association of long hodographs with large hail is also consistent with the modeling results of Dennis and Kumjian (2017), who found trajectories along the long axis of the storm, along which hail embryos could grow, were associated with larger hail.

5. Storm evolution

The following radar-based presentations and surface observations provide a basis for comparison between the 2021 April and October storms, and help to provide some insight as to why the April storm, which was sub-severe for most of ≈3 h after forming in southwest Oklahoma, transformed into a significant-hail-producing storm (MESH values of 50–75 mm or 1.9–2.9 in; although MESH may have underestimated hail size up to this point for reasons detailed in section 2), with a rapid change in intensity and morphology at 0100–0115 UTC at ≈30 mi (48.3 km) west of the center of Norman.

The MRMS 6-h hail swath (MESH values) at 0400 UTC for 29 April 2021 and 0400 UTC 11 October 2021 (Fig. 6, with 6-h, mid-level, 3–6-km, rotation track insets which show the maximum azimuthal shear in the layer; Heymsfield and Musil 1982 showed that radar-derived trajectories of the largest hail cyclonically traversed the periphery of the mid-level mesocyclone within the hail-growth zone; Witt 1998, Blair et al. 2017, Gutierrez and Kumjian 2021 and many others have shown the association of storm rotation with large hail) showed the April storm's hail swath (Fig. 6a) was considerably smaller horizontally than with the October storm (Fig. 6b). Of the 2021 storms in Norman, the April swath had the largest area of the largest MESH values (50–75 mm or 1.9–2.9 in), especially on the west side of Norman (although MESH could have under-estimated hail size, as detailed in section 2).

For the April storm, the swath portion with MESH values ≥10 mm (0.4 in) was 109 mi (177 km) long (Fig. 6a), and continuous swath length for MESH ≥50 mm (2 in) was about 14.2 mi (22.8 km). The largest MESH values were in the northern regions of Grady, McClain, and Cleveland counties (county names are shown in Fig. 6a in red), which is consistent with the 1.5–3.2-in (3.8–8.1-cm) hail reports in those areas (Table 1). In contrast, the October MESH values ≥10 mm (0.4 in) had length ≈164.4 mi (264.5 km; Fig. 6b), although only a few pixels indicated hail diameter ≥50 mm (2 in) in the Norman area. The largest MESH values for the October storm were in southwest Oklahoma, with a 23.5-mi (37.8 km)-long region of MESH values ≥50 mm (2 in). There were also smaller pockets with MESH of 75–100 mm (2.9–3.9 in) in southwest Oklahoma, yet only one significant hail report (≥2 in or 5.1 cm) from this region (2 in or 5.1 cm in Kiowa County). The population density in southwest Oklahoma is much less than in the Norman and Oklahoma City areas.

As suggested by the hail swaths, the April and October storms had remarkably similar tracks through Norman, although this might be somewhat less surprising given the similar mid- and upper-level flow directions and speeds shown in Fig. 4 with both storms. The April storm affected Norman almost exactly 1 h later than the October storm [sunset in Norman was at 0114 (0001) UTC on 29 April 2021 (11 October 2021)]. The tracks of the locations of the maximum reflectivity, using constant-altitude plan position indicator (CAPPI) at a height of 2000 m above radar level (ARL), were within ≈30 mi (48.3 km; Fig. 7) of each other. The tracks converged and crossed at ≈15.5 mi (25 km) west of the center of Norman. The April storm moved at ≈25–35 mph (11.2–15.6 m s^{-1}), while the October storm moved at ≈40–50 mph (17.9–22.4 m s^{-1}) and both storms accelerated as they approached central Oklahoma.

Considerable rain fell in Oklahoma in the overnight hours of 27–28 April 2021, with numerous flood reports associated with early morning convection (NCEI 2023c). Additional ongoing rainfall occurred in the vicinity of the surface wind-shift boundary, including in portions of Grady, McClain and western Cleveland Counties, with 12-h rainfall totals at 2300 UTC 28 April 2021 of 3–5 in (7.6–10.2 cm; Fig. 8a). Surface evaporation of previous rainfall perhaps enhanced a moisture gradient and thus, the associated baroclinic zone.

The April storm originated in southwest Oklahoma at ≈2130 UTC (Fig. 7) and evolved well behind the quasistationary surface wind-shift boundary or front (e.g., at ≈2330 UTC, the storm was ≈60 mi or 96.6 km behind the boundary; Fig. 8b) and closed in on the boundary as the storm tracked east-northeastward toward central Oklahoma (Figs. 8b–f). In fact, one can track the echo cluster (and oddly persistent attendant weaker echoes extending northwest of the storm; Fig. 8b–f) from which the April storm formed, all the way back to west-northwest of Lubbock, TX at around 1630 UTC (not shown), although the storm was discontinuous until about 2130 UTC.

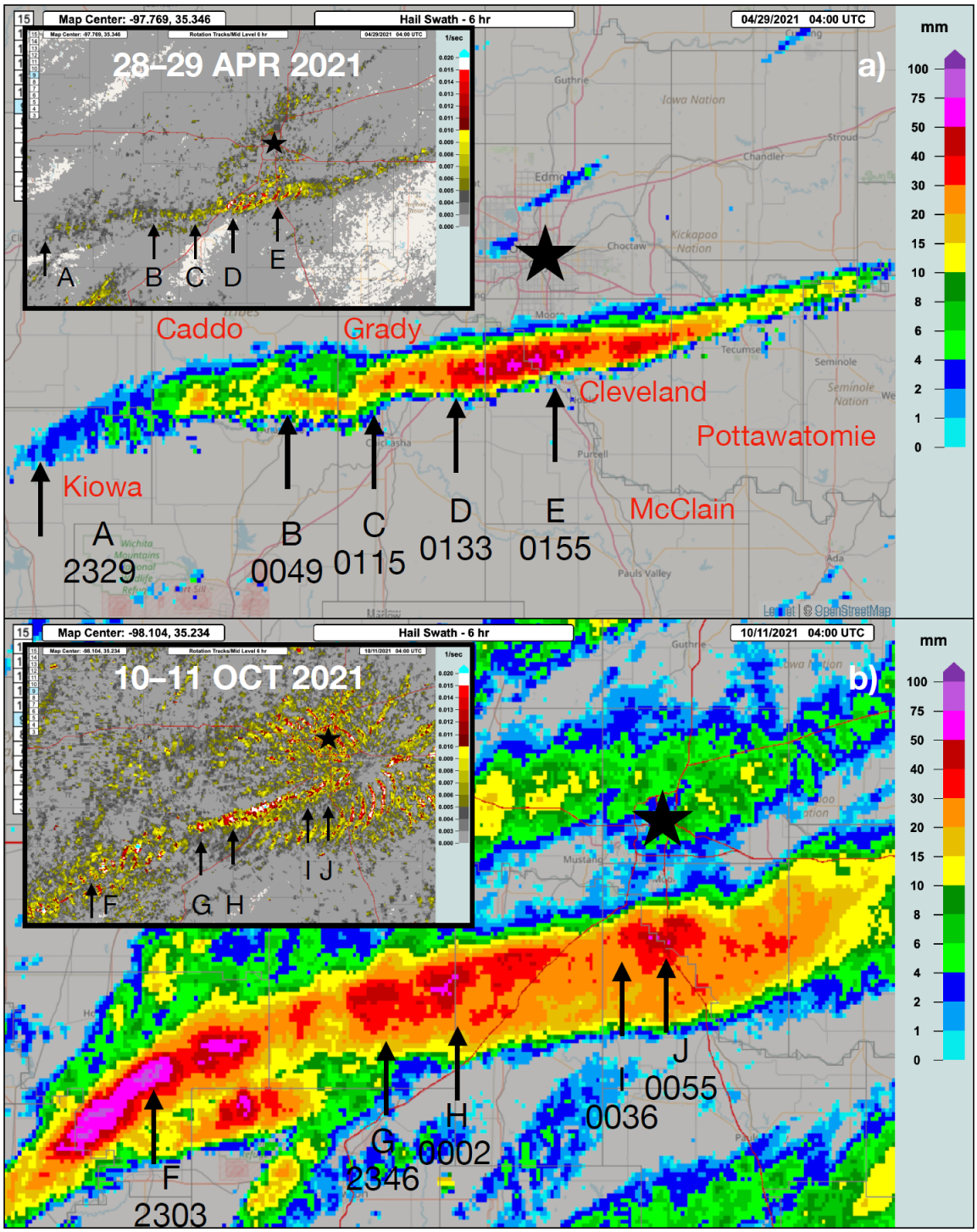

Figure 6: Multi-Radar Multi-Sensor (MRMS) maximum expected size of hail (MESH; Witt et al. 1998a) values (mm) over a 6-h period for: a) 2200–0400 UTC 28–29 April 2021 and b) 2200–0400 UTC 10–11 October 2021. Both panels are the same scale, but centered in slightly different locations. The star denotes Oklahoma City, OK ≈17.5 mi (28.2 km) north of Norman, OK. Insets show mid-level (3–6-km) MRMS rotation tracks (s^{-1}) for the same 6-h periods. Selected county names are shown in red font in (a). Black numeric labels are UTC times corresponding to those in Fig. 11; black arrows denote the east-west location within the swaths and rotation tracks of the maximum radar reflectivity at beam elevation 0.44˚ for the same times. *Click image to enlarge*.

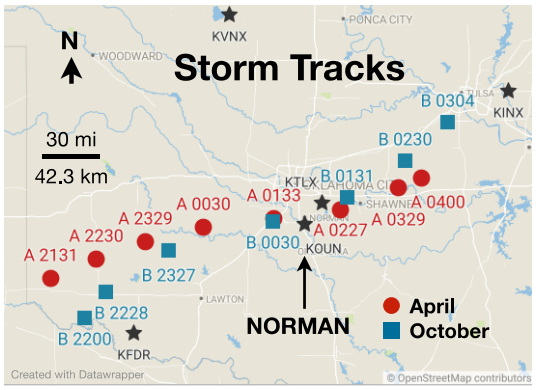

Figure 7: Locations and times (UTC) for 28–29 April 2021 (A; red dots) and 10–11 October 2021 (B; blue squares) of the visually estimated maximum reflectivity (using WCT software; NCEI 2023b) for each storm, via 2000-m ARL CAPPI. WSR-88D sites are black stars: KFDR (Frederick, OK; elevation 1267 ft or 386.2 m MSL), and KTLX (Oklahoma City, OK; elevation 1213 ft or 369.7 m MSL). Other sites noted are KINX (Tulsa, OK) radar, KVNX (Vance AFB, OK) radar and KOUN (Norman, OK) rawinsonde.

Once in Oklahoma, the echo cluster strengthened to reflectivity values of around 55 dB*Z* (using 2000 m ARL CAPPI), with 50-dB*Z* echo-tops at 2 km MSL, and a storm was established at ≈2130 UTC 28 April 2021 (Fig. 9a and 10a). The April storm had maximum reflectivity mostly less than mid-60s dB*Z*, and low values of mid-level 3–6-km rotation (Fig. 6a inset; <0.01 s^{-1}), from its formation until ≈0100 UTC 29 April 2021. There was a pocket of MESH 20–30 mm (0.79–1.2 in) in western Caddo County, OK, at 0016–0018 UTC 29 April 2021, after which MESH decreased (Fig. 6a).

At ≈0049 UTC (Fig. 6a location denoted with B; see also Figs. 10a; Fig. 11b), the MESH values showed a more continuous area of 20–30 mm (0.79–1.2 in). The 50-dB*Z* echo top increased from ≈8 to 10 km MSL, and 60-dB*Z* echo top from ≈4 to 5 km MSL (Fig. 9a). The radar presentations at 0049 UTC and 0115 UTC (Fig. 11b,c) also showed that the storm structure had begun to develop a much tighter inflow notch, a deep weak echo region (WER; ≈16 000 ft or 4.9 km; not shown for this time), and increased mid-level rotation (Fig. 6a, inset; rotation values ≥0.01 s^{-1} first identified at 0104 UTC). Notably, the April storm persisted for over 3 h, before developing mid-level rotation ≥0.1 s^{-1}.

By 0115 UTC 29 April 2021, the reflectivity values of the April storm increased to ≥70 dB*Z* (Fig. 10a; Fig. 11c) and MESH increased to 40–50 mm (1.6–1.97 in) at ≈0118 UTC (Fig. 6a, location denoted with C; could indicate a change from dry to wet hail and/or increase in hail size). Somewhat stronger mid-level (3–6-km) rotation (and low-level 0–2-km rotation, not shown) developed by ≈0133 UTC (Fig. 6a inset, location denoted by D; ≈0.02 s^{-1}). In accordance with the rapid intensification at ≈0110–0115 UTC, the vertically integrated ice (VII; a measure of lightning density; Gauthier et al. 2006) increased substantially at 0120 UTC, and the 50-dB*Z* over 0˚C and 60-dB*Z* over –20˚C layer thicknesses increased (Fig. 9a).

No Oklahoma hail reports were received until 0134 UTC on 29 April 2021 (Table 1). At 0128 UTC, the first severe thunderstorm warning was issued. At 0149 UTC a prominent WER appeared on the leading edge of the storm through at least ≈16 000 ft (4.9 km, which may have impacted MESH values; Fig. 12a; not all times and beam elevation angles were examined). The 50- and 60-dB*Z* echo tops reached maximum heights of ≈11 and ≈8 km, respectively, at 0150 UTC 29 April 2021 (Fig. 9a), just as the storm arrived near the city limits of Norman. With the storm seemingly at its peak intensity, the Norman Mesonet station measured a 69-mph gust (30.8 m s^{-1}; Fig. 8f) at 0200 UTC 29 April 2021.

One possible reason for the April storm's intensification at 0100–0115 UTC, in Grady County, was the potential existence of a weak baroclinic zone, enhanced by prior rainfall, with associated larger horizontal virtual temperature gradients and accompanying horizontal vorticity. This feature then could have been tilted by an updraft leading to an increase in storm rotation (Fig. 8a; e.g., Rasmussen et al. 2000). Another contributing factor to intensification might have been that the storm became close enough to the surface wind-shift boundary to benefit from enhanced convergence and lifting, as well as possibly being able to access surface parcels from ahead of the boundary (Fig. 8d–f).

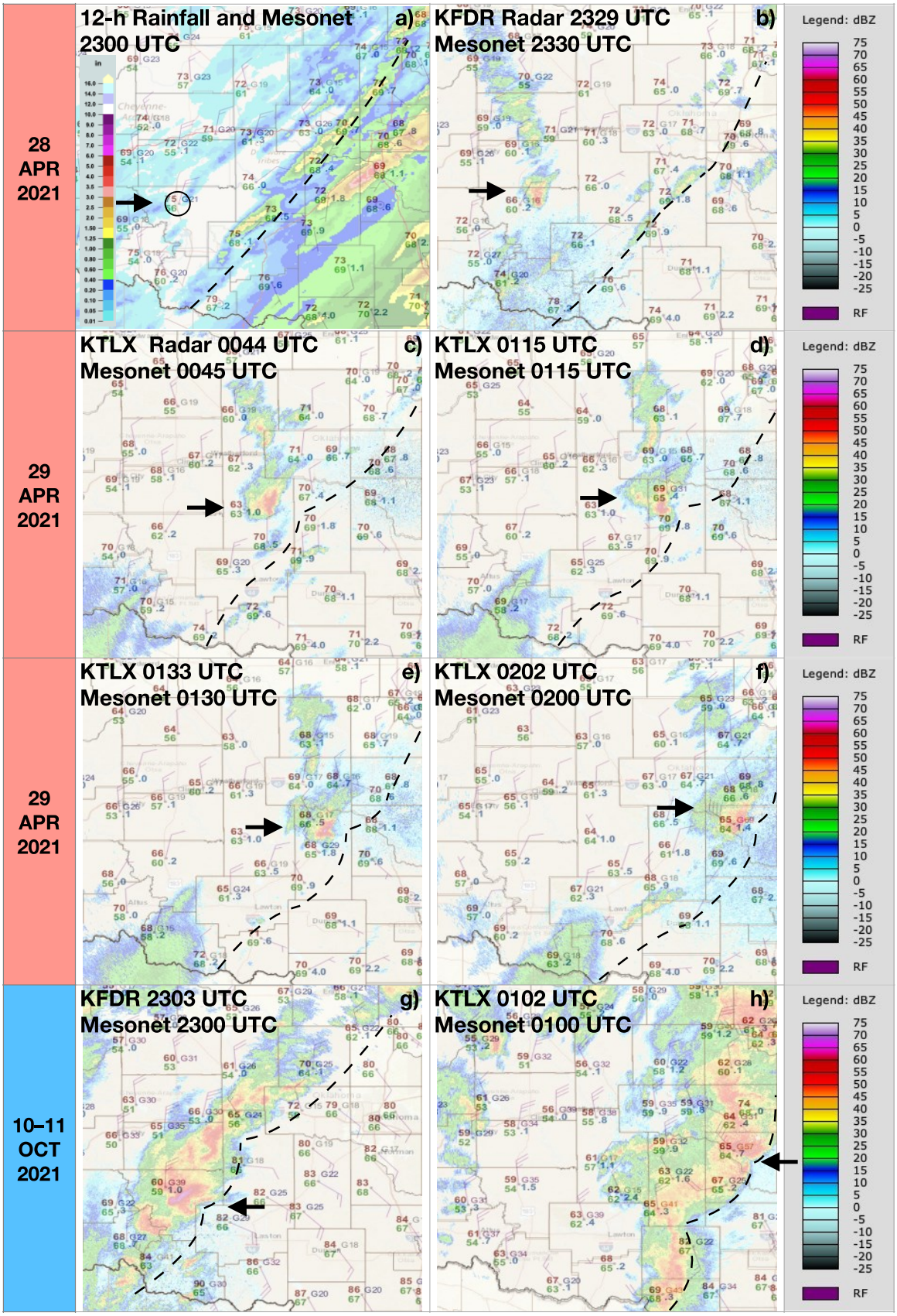
28 APR 2021
12-h Rainfall and Mesonet 2300 UTC
a)
KFDR Radar 2329 UTC
Mesonet 2330 UTC
b)
Legend: dBZ
75
70
65
60
55
50
45
40
35
30
25
20
15
10
5
0
-5
-10
-15
-20
-25
RF
29 APR 2021
KTLX Radar 0044 UTC
Mesonet 0045 UTC
c)
KTLX 0115 UTC
Mesonet 0115 UTC
d)
29 APR 2021
KTLX 0133 UTC
Mesonet 0130 UTC
e)
KTLX 0202 UTC
Mesonet 0200 UTC
f)
10–11 OCT 2021
KFDR 2303 UTC
Mesonet 2300 UTC
g)
KTLX 0102 UTC
Mesonet 0100 UTC
h)

Figure 8 *(previous page)*: Radar imagery and Oklahoma Mesonet surface observations overlain. a) MRMS 12-h rainfall Q3 multi-sensor, pass 2 (Zhang et al. 2016) and Oklahoma Mesonet surface observations overlain at 2300 UTC 28 April 2021. The circle denotes the location of the April storm at 2300 UTC. b)–f) 28–29 April 2021 and g)–h) 10–11 October 2021, radar reflectivity at beam elevation 0.44˚ and Oklahoma Mesonet surface station plots for selected times comparable to some of those in Figs. 6 and 11. (In this figure times shown are very close to, but do not exactly match the times shown in Figs. 6 and 11, in order to match the radar data with the selected 15-min intervals of the mesonet surface maps). Conventional station plot with temperature (red; ˚F), dewpoint (green; ˚F), and winds (pennant = 50 mph or 22.4 m s^{-1}; full barb = 10 mph or 4.5 m s^{-1}; half-barb = 5 mph or 2.2 m s^{-1}; gusts = G, magnitude in mph). Radar imagery from KFDR (Frederick, OK) and KTLX (Oklahoma City, OK). Black dashed line = approximate surface wind-shift boundary position. Black arrows indicate the hailstorm of interest.

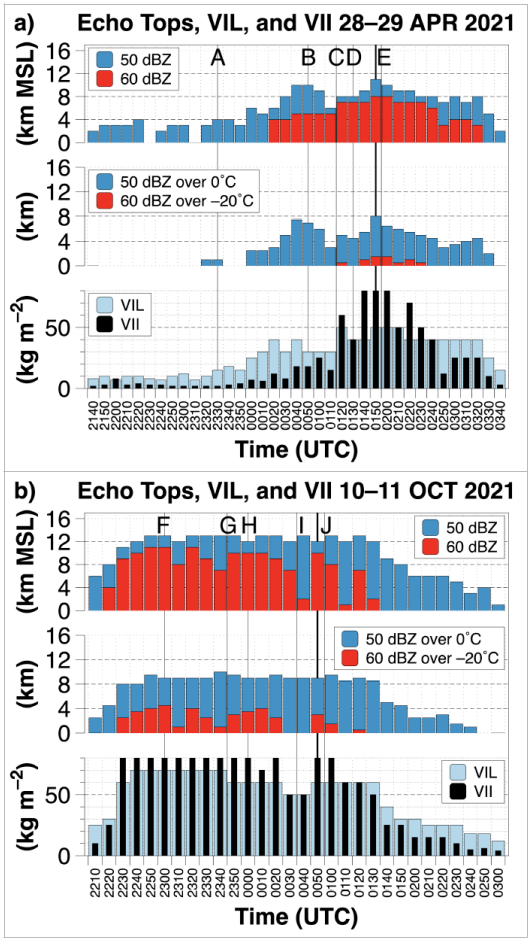

Figure 9: Echo-top heights (km MSL; top axes) for 50 dB*Z* (dark blue) and 60 dB*Z* (red); layer thickness (km; middle axes) of 50-dB*Z* echo top over 0˚C height (dark blue) and 60-dB*Z* echo top over –20˚C height (red); vertically integrated liquid (VIL; kg m^{-2}; bottom axes; light blue), and vertically integrated ice (VII; kg m^{-2}; bottom axes; black) for a) 28–29 April 2021 and b) 10–11 October 2021. All quantities visually estimated from MRMS. Maximum value for an MRMS value bin is shown; e.g., for echo height 8–9 km, the height plotted is 9 km and the selected maximum is chosen from anywhere within the storm of interest at a given time. The MRMS VII values for the bin with VII >70 kg m^{-2} were set equal to 80 kg m^{-2} for plotting purposes. Capital letters correspond to the times shown in Fig. 6, with bold vertical black line denoting the approximate time that the storm affected Norman, OK. Time interval was 10 min. Starting time is of the first non-zero 50-dB*Z* echo height. *Click image to enlarge*.

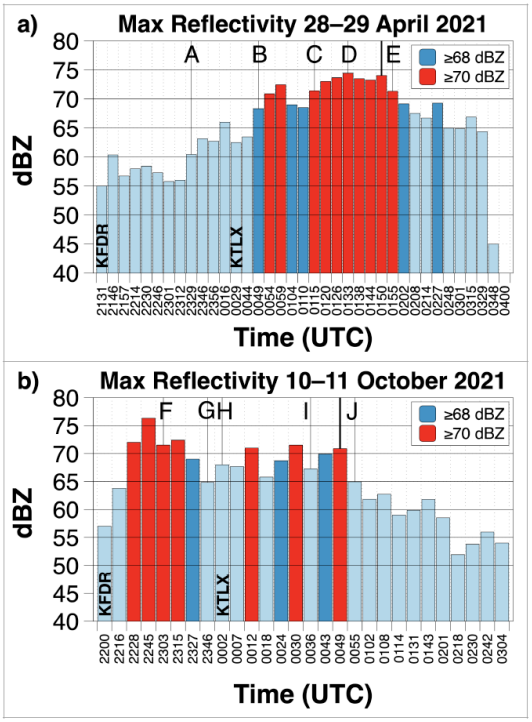

Figure 10: Maximum radar reflectivity (>40 dB*Z*; evaluated with WCT software; NCEI 2023b) using ARL CAPPI 2000 m from KFDR and KTLX. Labels on the vertical bars denote first time of each radar use. for a) 28–29 April 2021 and b) 10–11 October 2021. Capital letters correspond to the times shown in Fig. 6, with bold vertical line denoting the approximate time that each storm affected Norman, OK. Times shown are every ≈15 min, except from 0044–0214 UTC for 28–29 April 2021 and from 0002–0114 UTC for 10–11 October 2021, where the interval is 5–6 min *Click image to enlarge*.

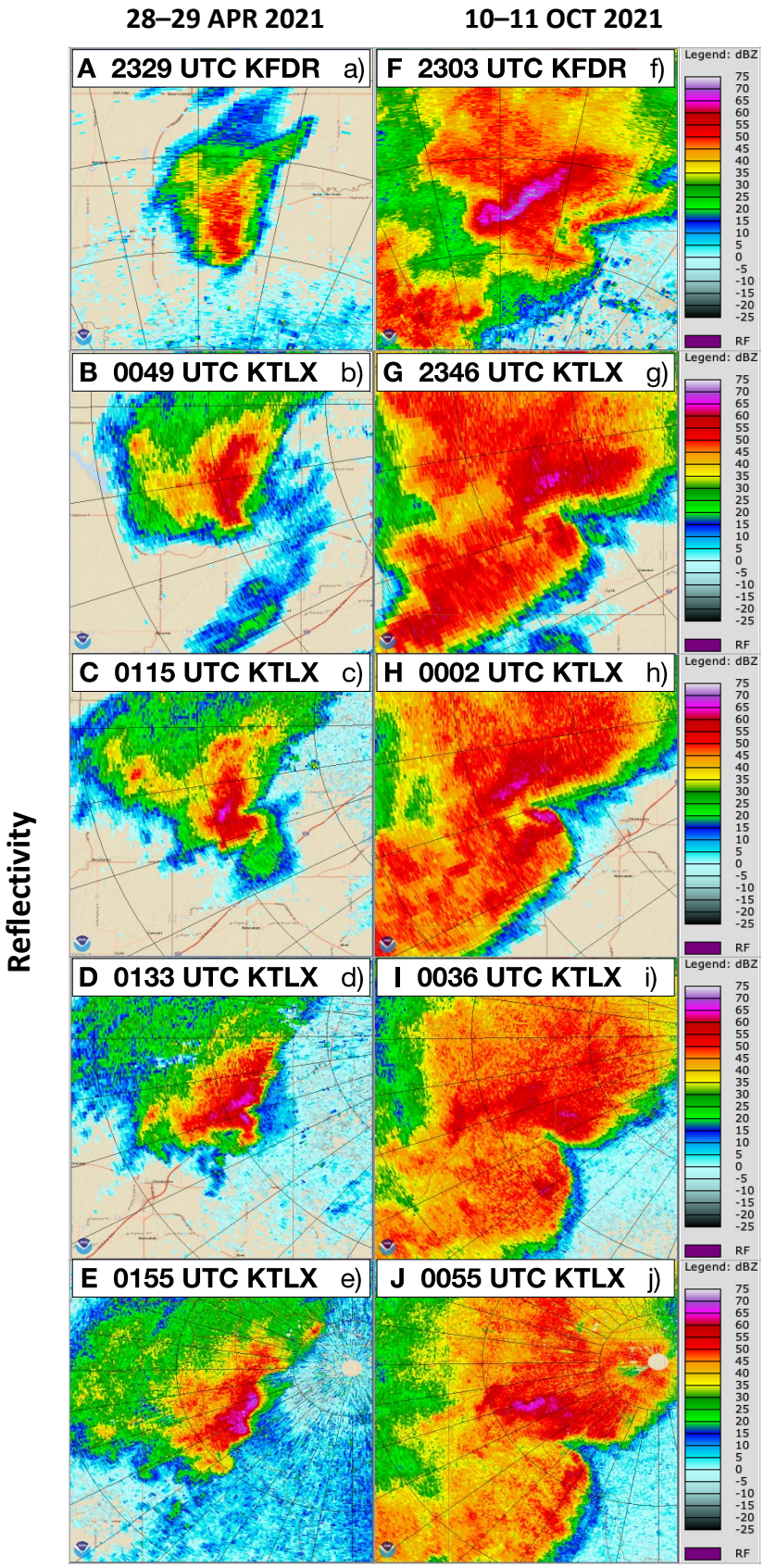
28–29 APR 2021
10–11 OCT 2021
Reflectivity
A 2329 UTC KFDR a)
F 2303 UTC KFDR f)
B 0049 UTC KTLX b)
G 2346 UTC KTLX g)
C 0115 UTC KTLX c)
H 0002 UTC KTLX h)
D 0133 UTC KTLX d)
I 0036 UTC KTLX i)
E 0155 UTC KTLX e)
J 0055 UTC KTLX j)
Legend: dBZ
75 70 65 60 55 50 45 40 35 30 25 20 15 10 5 0 -5 -10 -15 -20 -25
RF

Figure 11 *(previous page)*: Radar reflectivity at beam elevation 0.44˚ (0.45˚ for panel j) for the 28–29 April 2021 storm (left) and the 10–11 October 2021 storm (right). Capital letters in the upper left-hand corner of each panel correspond to the positions and times indicated by the same capital letters shown in Fig. 6. In each panel, the storm is roughly centered in the frame. The top-row images are from KFDR (Frederick, OK) and all other panels are from KTLX (Oklahoma City, OK). Range rings are every 20 km and spokes are every radial 10˚. *Click image to enlarge.*

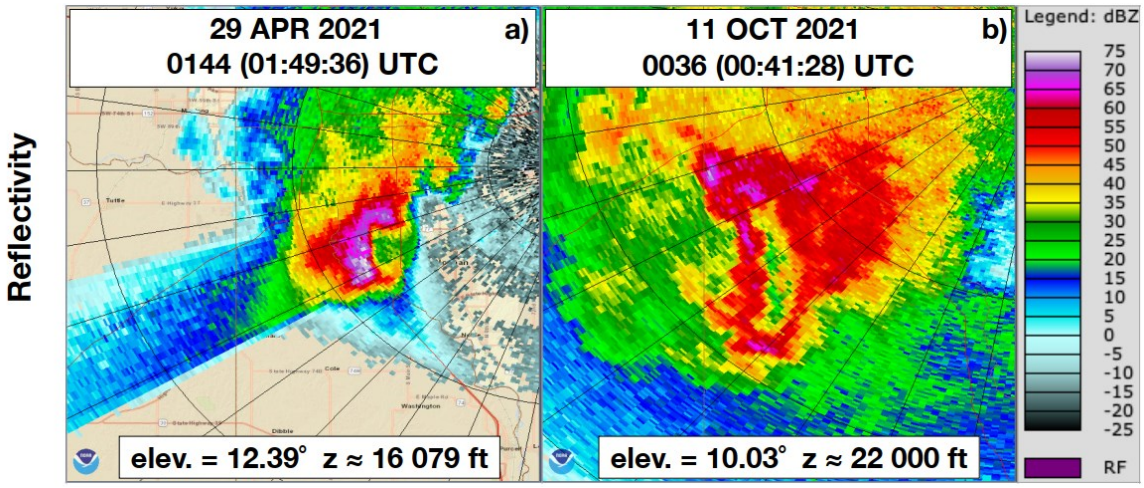

Figure 12: Radar reflectivity from KTLX (Oklahoma City, OK) showing weak-echo regions (WERs) for a) 28–29 April 2021 (beam elevation 12.39˚) and b) 10–11 October 2021 (beam elevation 10.03˚). Height *z* is the approximate height of the WER in each panel. Times shown in the titles are the time of the first radar sweep in the file for that time, and in parentheses is the time of the sweep shown in each panel for the given beam elevation. Range rings are every 20 km and spokes are every radial 10˚. *Click image to enlarge*.

Storms behind boundaries are often elevated, and in some environments, can be associated with large hail (Grant 1995; Moore et al. 1998; Horgan et al. 2007; MacIntosh and Parker 2017). However, the April storm was likely not elevated, based on the lack of a boundary-layer inversion, and on small mixed-layer convective inhibition (MLCIN) values of –22 to 0 J kg^{-1} from HRRR model-derived soundings from about 2200–0000 UTC 28–29 April 2021 at locations southeast (within 35 mi or 56.3 km) of the April storm track (not shown). Note that model CIN values tend to be underestimated; also, MLCIN = 0 J kg^{-1} at KOUN 29 April 2021 0100 UTC HRRR F000 (Fig. 5, Table 2). These model soundings were not characteristic of elevated-storm environments, as compared with typical elevated-storm profiles that exhibit strong inversions (e.g., Horgan et al. 2007). In addition, Nowotarski et al. (2011) showed that almost all simulated elevated storms had some parcels with near-surface origins, such that even if the April storm were elevated, it could have had access to surface parcels.

The evolution of the October storm was considerably different from that of the April storm, in that the former was associated with at least seven reports of tornadoes (Table 1), much stronger rotation characteristics (Fig. 6b inset), and eventually, mesoscale convective vortex characteristics (MCV; e.g., Davis and Weisman 1994) as it approached Norman (Fig. 11f–j). In addition, the October storm originated near, or possibly even along, a surface boundary (Fig. 8g,h) in southwest Oklahoma, and moved east-northeastward, roughly along the boundary.

The 10–11 October 2021 storm structure (Fig. 11f–j), 6-h MESH values (Fig. 6b), and mid-level rotation track (Fig. 6b, inset) showed that the October storm was much larger in area than the April storm, had a very prominent inflow notch, and a BWER (Fig. 12b) aloft when approaching Norman at ≈0041–0055 UTC 11 October 2021. That large BWER (Fig. 12b) could have resulted in the underestimation of hail sizes, based on MESH and the fact that only a few pixels indicating diameter ≥50 mm (2 in) were present near Norman (Fig. 6b).

The largest maximum reflectivity values for the October storm (≈76 dB*Z*; Fig. 10b) and highest 60-dB*Z* echo-top heights (11 km MSL; Fig. 9b) occurred in southwest Oklahoma, early in the storm's lifetime, where 2-in (5.1-cm) hail was reported (Table 1). As stated previously, the decrease in reflectivity values as the storm moved toward central Oklahoma could reflect a previously wet-hail dominant phase when the storm was in southwest Oklahoma, shifting to more of a dry-hail phase when the storm approached Norman.

The maximum reflectivity decreased somewhat at ≈2320–0000 UTC 10–11 October 2021 (Fig. 10b), approximately during tornado times, 2259–0016 UTC, (including an EF2 at 2345 UTC; Table 1), but increased sporadically to ≥70 dBZ at 0012 UTC, 0030 UTC, and at 0049 UTC, just prior to the storm's arrival in Norman. No hail was reported during the tornado times, which might represent a situation where only the most severe event was reported (Morgan and Summers 1982); however, between ≈2300–0000 UTC, MESH values were ≈40–50 mm (1.6–1.97 in), indicating the possibility of severe hail. [Although tornado development is not the focus of the current study, Snook and Xue (2008) found a decrease in evaporation of water and melting of hail (e.g., dry hail phase) led to weaker cold-pool development and an increased tornado risk, while the opposite was found with an increase in evaporation of water and melting hail (e.g., water-coated hail phase), which led to stronger cold-pool development and a decreased chance of tornadogenesis.] Lastly, the Norman mesonet measured a 57-mph (25.5-m s^{-1}) gust at 0100 UTC 11 October 2021, associated with the storm passage (Fig. 8h).

In summary, the April storm developed well behind a surface wind-shift boundary at about 2130 UTC 28 April 2021 in extreme southwest Oklahoma, became close enough to possibly interact with the boundary at around 0100–0115 UTC 29 April 2021, and dissipated around 0345–0400 UTC 29 April 2021, after travelling about 200 mi (322 km) over ≈6.5 h (Fig. 7). The 10 October 2021 storm also began in southwest Oklahoma, but near or with a surface front, starting at about 2200 UTC, and was no longer discretely identifiable (became part of a more linear convective mode) by about 0300 UTC 11 October 2021, while travelling a distance of about 215 mi (345 km) over ≈5 h (Fig. 7). Both were long-lived, isolated storms. The April storm at times (mainly near and after 0100 UTC) resembled a supercell, based on mid-level rotation values and other characteristics. The October storm clearly resembled a supercell from formation until well after Norman.

6. Polarimetric signatures

Polarimetric signatures, using 2000 m ARL CAPPI, are presented next, to: 1) help support documentation presented in the previous section of the rapid intensification of the April storm between 0100–0115 UTC 29 April 2021 (Fig. 13, left column, 0029 UTC 29 April 2021, a time prior to the intensity increase; Fig. 13 middle column, 0144 UTC 29 April 2021, a time after the intensity increase); 2) to examine hail signatures at 0043 UTC on 11 October 2021 (Fig. 13, right column) for the October storm; and 3) make comparisons of polarimetric radar appearance and likely hail characteristics between the two 2021 storms of interest.

At 0029 UTC 29 April 2021, there were two local maxima in reflectivity (Fig.13a; 2000-m ARL CAPPI) for the April storm: one to the north and one to the south of the storm's indentation on the east leading edge. Only a few pixels had reflectivity values ≥60 dB*Z*, with maxima of 62.5 dB*Z* in the northern portion of the storm and 62.0 dB*Z* in the southern portion. The differential reflectivity (Z_{dr}) values (Fig. 13b) were mostly positive in the ≥55 dB*Z* region, with a isolated single pixels of –0.20 dB and –0.36 dB in the southern portion of the storm, both in 57 dB*Z*, with cross-correlation coefficient, ρ_{hv} (Fig. 13c) of 0.87 and 0.72, respectively. This likely indicated small wet hail (d <20 mm or 0.79 in) mixed with heavy rain (Straka et al. 2000). Such low ρ_{hv} values could indicate a few hailstones with large protuberances, or highly oblate stones. A few pixels of Z_{dr} ≤–1.5 dB in ≥55-dB*Z* reflectivity, with ρ_{hv} of 0.969, appeared near the southeast leading edge of ≥55-dB*Z*, although these were located within a reflectivity gradient which can impact Z_{dr} accuracy. In summary, at 0029 UTC, the polarimetric signatures of the April storm possibly indicate some <1-in (2.54-cm) hail at a few pixels in the southern portion of the storm, with primarily rain elsewhere.

In contrast, at 0144 UTC 29 April 2021, the maximum reflectivity (Fig. 13d; 2000-m ARL CAPPI) values and area covered by ≥60 dB*Z* had increased markedly. Southern and northern regions had local reflectivity maxima

of 72.3 dBZ in the south and 73.3 dBZ in north, with the former (latter) containing the minimum (secondary minimum) Z_{dr} value (Fig. 13e) of –5.3 (–3.3) dB in 66.4- (67.4-) dBZ reflectivity, and ρ_{hv} (Fig. 13f) of 0.820 (0.826) at the minimum Z_{dr} location(s). These Z_{dr} minima in both the north and south regions were located within broader regions of substantially negative (≤–2 dB) Z_{dr}, with the southern region containing very low (<0.9) ρ_{hv} values. In general, at 0144 UTC, the Z_{dr} and ρ_{hv} values were much lower than at 0029 UTC, consistent with much larger hail (40–50 mm or larger; Balakrishnan or Zrnić 1990; Straka et al. 2000) covering a larger area. Hail with diameter ≥50 mm (1.97 in), which is a Mie scatterer for ≈11-cm radar, can produce a wide range of reflectivity values 60–80 dBZ, Z_{dr} ≤–2 dB, and ρ_{hv} <0.9 (Balakrishnan and Zrnić 1990; Straka et al. 2000). Note that a 2.75-in (7-cm) hail report was received at 0144 UTC 29 April 2021, located 2 mi (3.2 km) north-northeast of Blanchard, OK, nearest the southern portion of the storm (Table 1).

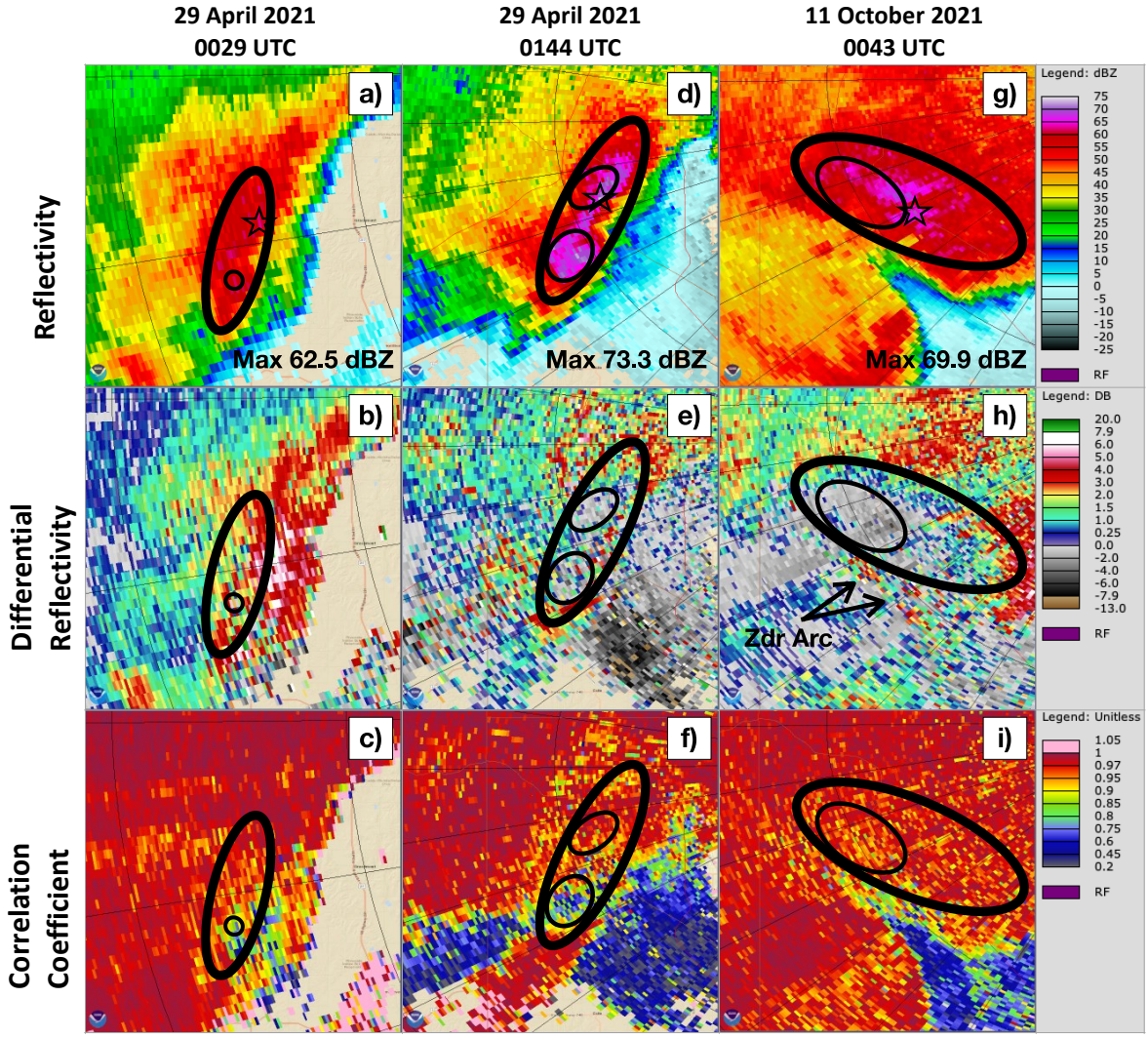

Figure 13: Radar reflectivity (dBZ; top), differential reflectivity (Z_{dr}, dB; middle row), and cross-correlation coefficient (bottom row) for 0029 UTC 29 April 2021 (left), 0144 UTC 29 April 2021 (middle column), and 0043 UTC 11 October 2021 (right) using 2000-m ARL CAPPI from KTLX (Oklahoma City, OK). Open stars denote the locations of the maximum reflectivities with numeric values in black. Heavy outline ovals denote the approximate region of highest reflectivities (≥55–60 dBZ), and thinner outline ovals denote the approximate regions of the locally lowest Z_{dr} values. Range rings are every 20 km and spokes are every radial 10˚. *Click image to enlarge.*

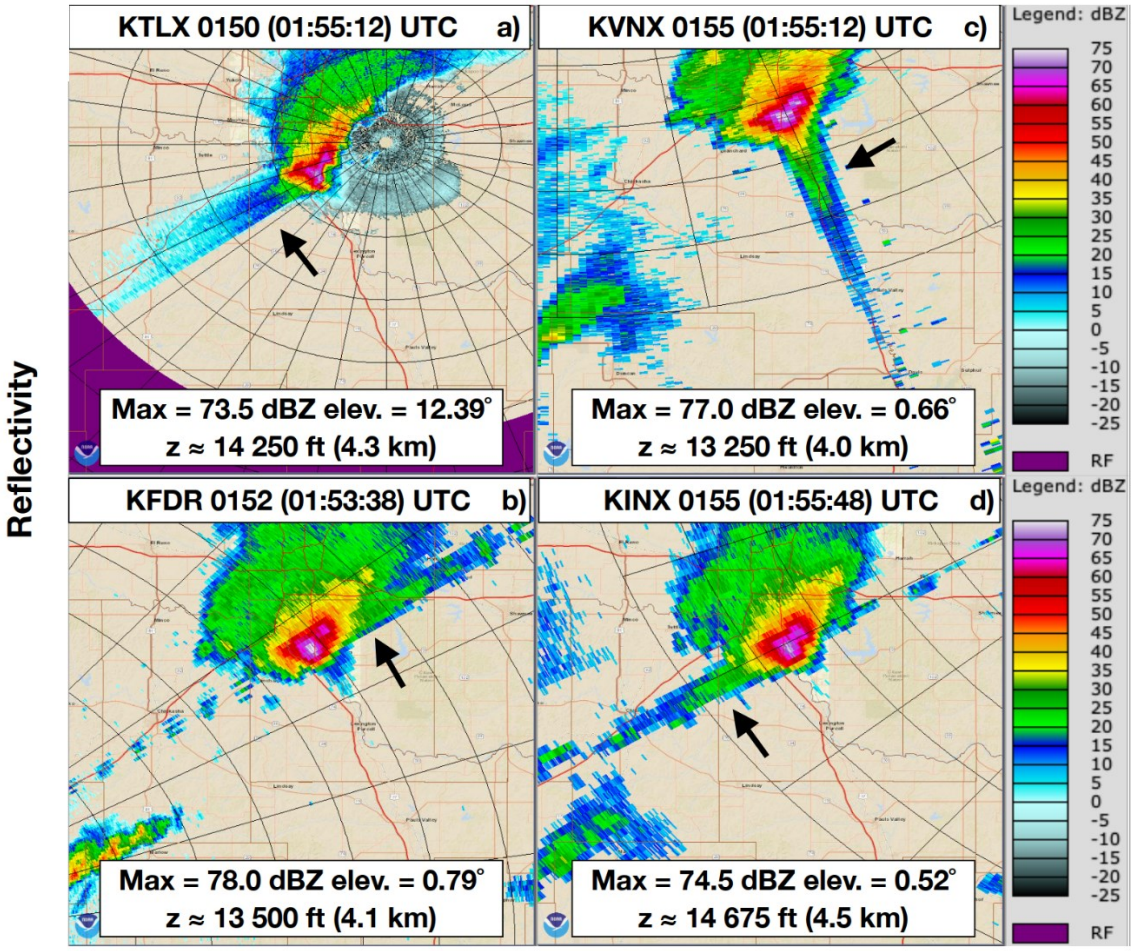

Figure 14: Radar reflectivity with a three-body scatter spike (TBSS) from the 28–29 April 2021 storm from (Oklahoma City, OK), b) KFDR (Frederick, OK), c) KVNX (Vance AFB, OK), and d) KINX (Tulsa, OK),, with local maximum reflectivity for each panel at approximately similar heights, *z*. Times shown in the titles represent the first radar sweep in the file for that time. In parentheses is the time of the sweep shown in each panel for the given beam elevation. For display purposes, (c) has a more southward center from the other panels. Radar locations noted in Fig. 7. Range rings are every 20 km and spokes are every radial 10˚. *Click on image to enlarge*.

The polarimetric signatures at 0144 UTC substantiate the rapid increase in hail size and storm intensity of the April storm after ≈0100–0115 UTC, documented previously (Figs. 6a, 9a, 10a, and 11).

In comparison, at 0043 UTC 11 October 2021, the October storm's reflectivity region of values ≥55 dB*Z* (Fig. 13g; 2000-m ARL CAPPI) covered a much larger area than that of the April storm at any time, with a core of highest reflectivity located on the forward flank, north of the well-developed inflow notch. The maximum reflectivity at 0043 UTC was 69.9 dB*Z*. Negative Z_{dr} (Fig. 13h) values covered a much larger single area than was the case for the April storm, with minimum Z_{dr} for the October storm of –6.18 dB in 58-dB*Z* reflectivity, with ρ_{hv} (Fig. 13i) of 0.952, indicating possible large wet hail (d >20 mm or 0.79 in; Straka et al. 2000). The broader area of negative Z_{dr} values in the forward flank was offset slightly to the west-southwest of the region of highest reflectivity ≥60 dB*Z* (such offsets have been noted by Kumjian and Ryzhkov 2008 and Picca and Ryzhkov 2012).

The ρ_{hv} values in the broader region of negative Z_{dr} values at 0043 UTC 11 October 2021 (Fig. 13 right column) were not as low as for the April storm at 0144 UTC 29 April 2021 (Fig. 13 middle column), ranging mostly from about 0.849–0.97, but still indicated the possibility of very large hail (diameter >40 mm

or 1.6 in; Balakrishnan and Zrnić 1990). A 1.75-in (4.4-cm) hail report appeared at 0040 UTC, 4 mi (6.4 km) northeast of Blanchard (Table 1). The narrow region of large positive Z_{dr} values (≈3–6.7 dB) along the leading edge of the storm might be evidence of a Z_{dr} "arc" (Kumjian and Ryzhkov 2008), as it was positioned on the southern edge of the forward flank downdraft and existed in an environment with a 0–1-km SRH value of 183 m^2 s^{-2}.

Near Norman, the hail reports for the April storm were generally larger (1.75–3.2 in or 4.4–8.1 cm; mean 2.2 in or 5.6 cm; Table 1) than those in October (1–3 in or 2.5–7.6 cm; mean 1.7 in or 4.3 cm; Table 1). Balakrishnan and Zrnić (1990) and Straka et al. (2000) have discussed that ρ_{hv} can be smaller in regions where hailstones have prominent protuberances (compare Fig. 13f and Fig. 13i), such as those associated with the April storm (Fig. 2b), in contrast to the somewhat higher (but still low) values of ρ_{hv} and smoother hailstones associated with the October storm (Fig. 2d). Large reflectivity with ρ_{hv} <0.9 can signal oblate hailstones >50 mm (1.97 in) with small protuberances. A caveat is that there may also have been hailstones associated with each storm with different degrees of protuberances than the ones in Fig. 2. Mie scattering effects make discerning more precise hail sizes difficult at best.

Finally, a very prominent and persistent three-body scatter spike (TBSS), often associated with large hail (e.g., Zrnić 1987; Picca and Ryzhkov 2012), was detectable at multiple levels, nearly continuously for almost 2 h with the April storm, starting at about 0049 UTC (very prominent after about 0138 UTC) in Caddo County until about 0248 UTC, when the storm was near Shawnee, OK. Remarkably, likely due to the isolation of the April storm from any other radar echoes, the TBSS with the April storm was identifiable from at least four different Oklahoma radars at ≈0155 UTC 29 April 2021 and a height of about 13 000–15 000 ft (4.0–4.6 km; Fig. 14), where maximum reflectivity values were as high as 78 dB*Z*: KTLX, KFDR, KVNX, and KINX. [The TBSS, although a bit less pronounced, also could be detected from KICT (Wichita, KS) at 0155 UTC and KSRX (Fort Smith, AR) at 0154 UTC]. Lastly, the TBSS first detected at about 0049 UTC 29 April 2021, from KTLX at beam elevation 3.03˚ (not shown), was roughly consistent with the timing of that storm's rapid intensification.

There was also a TBSS with the October storm, identified from KTLX, at 0049 UTC 11 October 2021 at beam elevation 15.6˚, with maximum reflectivity of 74.5 dB*Z* at a height of about 24 854 ft (7.6 km; not shown). The TBSS also was evident at 0036 UTC at 30 000 ft (9.1 km), but it was only found at very high heights (≥25 000 ft or 7.6 km), and only at a couple of sampled times, although not all times and beam elevation angles were explored.

7. Comparison with other 3-in (7.6-cm) hailstorms in Cleveland County

Next, we present a cursory comparison of proximity sounding parameters and radar presentations of two 2021 storms of interest with those of the previous (prior to 2021) six dates, on which a total of 12 reports of hail ≥3-in (7.6-cm) were received, for Cleveland County from 1955–2021 (Table 2; a larger region with larger sample size is being considered for a future study; one 3-in or 7.6-cm hail report from 28 April 1956 was stated to be in Cleveland County, but the latitude and longitude location were in McClain County and thus, this case is not included; Figs. 15–16).

For several of the Cleveland County ≥3-in (7.6-cm) hail dates, the time difference between (completed/at least to the EL) available observed soundings and the time of the maximum ≥3-in (7.6-cm) hail reports was >4 h. In these cases, model-derived soundings were selected as proximity soundings. Specifically, the latitude and longitude of KOUN were used to generate North American Regional Reanalysis, (NARR; 32-km horizontal resolution and 3-h temporal output resolution; Mesinger et al. 2006; Northern Illinois University 2023) model soundings for KOUN 04 May 1999 0000 UTC and KOUN 20 May 2010 0000 UTC; the North-American Mesoscale Analysis and Forecast System–nested model (NAMnest; 3-km horizontal grid resolution and 6-h temporal output resolution; EMC 2023) was used for KOUN 19 May 2013 2100 UTC F003 (forecast hour three); and the HRRR model was used for KOUN 04 May 2020 2100 UTC and KOUN 29 April 2021 0100 UTC, each at F000 (forecast hour zero). All sounding-derived quantities were obtained using SHARPpy (Blumberg et al. 2017). All the Cleveland County

cases of 3-in (7.6-cm) hail reports occurred in the months of April or May, except for the 10–11 October 2021 case.

The 10 May 2010 (2010a) sounding was very potent in terms of both buoyant instability and shear, and perhaps not surprisingly, was associated with the largest hail report (4.6 in or 11.7 cm) of these Cleveland County hail cases. The 2010a date had the largest LHP of 41.6 and SHIP of 2.6 (2nd largest after SHIP of 4.0 on 04 May 1999). However, overall, the April and October 2021 dates had some of the largest deep shears and also the lowest CAPE values (Fig. 15). In particular, as compared with the other Cleveland County cases, the April and October 2021 dates together, had: lowest MUCAPE, lowest MLCAPE, lowest MUEL, lowest MLEL, lowest SHIP values, highest –30˚C heights, and thickest HGZ depths (JS14 showed an association of shallower HGZ depths with increasing hail size). Moreover, except for the 2010b date, the two 2021 cases had the highest PW. Additionally, except for the 2010a date, the April and October 2021 cases had the largest 0–6-km shear; third and first-largest 0–8-km shear, respectively; largest EBWD; and highest 0–EL shear (Table 2).

Individually, the April date had some anomalous lowest values when compared with the other Cleveland County cases. These were: MULCL, SCP, 0–1-km SRH (the only negative value); 0–3-km SRH, effective SRH; effective shear; SSP; SHIP; and LHP. The April date also had the lowest 0–3-km shear value. Thus, in the presence of weaker buoyancy, larger deep shear (and not necessarily larger lower-level shear, which is important for supercells and tornadoes) apparently can compensate for the production of significant hail (NA22 state that shear above 1 km was important for severe hail).

An approximate inverse relationship between the CAPE and shear parameters can be identified roughly for these eight cases (Fig. 15; keeping in mind the small sample size), which supports the notion that for large hail, either CAPE or shear can compensate for lack of the other (e.g., Johns et al. 1993; NA22). Hodographs for these Cleveland County 3-in (7.6-cm) hailstorms were long hodographs for the two 2021 storms (Fig. 5) and the 1967 and 2010a cases (not shown), but the 1967 and 2010a soundings also had large CAPE (MUCAPE ≥3000 J kg^{-1}).

Nixon and Allen (2022) point out a possible difference between significant tornadic environments and significant hail environments: the 0–1-km bulk wind difference is typically <29.9 kt (15.4 m s^{-1}) for the latter, which is satisfied by all the Cleveland County ≥3-in (7.6-cm) hail sounding cases, despite four (six) of the hailstorms (hailstorm clusters) also being associated with tornadoes, all but two of which were significant, ≥F/EF2. However, these might not be proximity soundings for the tornado times in all cases. It is unknown if the 1967 tornado report was associated with the same storm as the 3-in or 7.6-cm hail report. Craven and Brooks (2004) also found 0–1-km bulk shear was lower for significant hail/wind events than for significant tornadic events. Additionally, the 700–500-hPa lapse rates exceeded 6.5˚C km^{-1} (JS14 for ≥2-in or 5.1-cm hail) for all but two (1967 and 2010b) of the Cleveland County cases.

Table 2 *(next page)*: Observed and model-derived sounding data (HRRR, NAMnest, from SHARPpy; NARR from Northern Illinois University 2023) from KOUN (KOKC for 1967) associated with the environments of ≥3-in (7.6-cm) hailstorms that affected Cleveland County from 1955–2021. All hail reports were located ≤15.84 mi (25.5 km) from the sounding locations. "Tornado on date" row indicates if a tornado occurred on the same date as the Cleveland County maximum hail report, and if it occurred with the same storm as the ≥3-in (7.6-cm) hail reports. Several tornado reports (including an EF2; Table 1) were associated with the October storm (Table 1), and the last one prior to the storm affecting Norman is listed in this Table. The 11 October 2021 0000 UTC observed sounding values were obtained from University of Wyoming (2023; observed data from 2021 was unavailable through the SHARPpy software interface at the time when this data was compiled), which was input to, and processed with SHARPpy. All sounding-derived quantities for all soundings were produced by SHARPpy for consistency (except 0–EL shear, THK_{HGZ}, $GRW\alpha_{EL}$, $SRW\alpha_{Mid}$, LHP, and LHP-related terms, A and B, which were calculated by the authors). Terms and acronyms are defined in Appendices A and B.

	1967 APR 17 0000 UTC OBS	1999 MAY 04 0000 UTC NARR	2010a MAY 10 2100 UTC OBS	2010b MAY 20 0000 UTC NARR	2013 MAY 19 2100 UTC NAMnest F003	2020 MAY 04 2100 UTC HRRR F000	2021a APR 29 0100 UTC HRRR F000	2021b OCT 11 0000 UTC OBS
Tornado on Date	F2 Seminole County,OK 0240 UTC	F5 same storm, 2326 UTC	EF4, same storm, 2220 UTC	EF1, same storm cluster, 0217 UTC	EF4, same storm cluster, 2301 UTC	EF1, same storm, 2250 UTC	None after 1200 UTC 28 April 2021	EFU same storm, 0016 UTC
MaxSz in (cm)	3.0 (7.6)	3.0 (7.6)	4.6 (11.7)	3.0 (7.6)	3.0 (7.6)	3.41 (8.7)	3.2 (8.1)	3.0 (7.6)
Hail Rprt (UTC)	0120	0028	2225	0034	2230	2242	0212	0104
MUCAPE (J kg^{-1})	3247	5377	3700	3944	3659	4135	1306	1932
MUCIN (J kg^{-1})	–24	0	–33	0	0	–1	–7	–27
MULCL (m)	974	627	630	847	1349	1989	276	1020
MULFC (m)	1573	627	2386	847	1349	2110	486	3313
MUEL (m)	12 566	12 410	12 851	12 614	12 597	13 256	11 232	11 724
MLCAPE (J kg^{-1})	2746	3943	3202	2918	3212	3218	915	1617
MLCIN (J kg^{-1})	–22	–1	–56	–1	–2	–19	0	–30
MLLCL (m)	1207	885	694	1116	1378	2154	579	1217
MLLFC (m)	1626	935	2515	1167	1514	2561	632	3313
MLEL (m)	12 566	12 059	12 668	11 920	12 420	13 110	10 833	11 237
PW in (cm)	1.27 (3.2)	1.05 (2.7)	1.15 (2.9)	1.78 (4.5)	1.34 (3.4)	1.09 (2.8)	1.47 (3.7)	1.53 (3.9)
LowRH (%)	67	77	89	70	65	44	92	70
MidRH (%)	59	29	27	98	45	32	76	62
$LR_{8–5}$ (˚C km^{-1})	7.2	7.7	6.7	7.0	7.5	8.1	6.4	7.1
$LR_{7–5}$ (˚C km^{-1})	6.4	8.3	7.8	6.4	8.0	7.9	7.3	8.2
0–1SRH (m^2 s^{-2})	116	155	312	105	85	71	–47	183
0–3SRH (m^2 s^{-2})	132	288	422	157	128	132	78	255
EffSRH (m^2 s^{-2})	121	169	368	164	142	105	22	246
0–1Sh kt (m s^{-1})	15 (7.7)	20 (10.3)	29 (14.9)	14 (7.2)	11 (5.7)	11 (5.7)	12 (6.2)	20 (10.3)
0–3Sh kt (m s^{-1})	43 (22.1)	30 (15.4)	61 (31.4)	28 (14.4)	35 (18.0)	39 (20.1)	16 (8.2)	41 (21.1)
EffSh kt (m s^{-1})	26 (13.4)	22 (11.3)	37 (19.0)	35 (18.0)	27 (13.9)	24 (12.3)	6 (3.1)	36 (18.5)
0–6Sh kt (m s^{-1})	46 (23.7)	37 (19.0)	76 (39.1)	39 (20.1)	48 (24.7)	35 (18.0)	67 (34.5)	71 (36.5)
0–8Sh kt (m s^{-1})	73 (37.6)	47 (24.2)	81 (41.7)	42 (21.6)	49 (25.2)	39 (20.1)	76 (39.1)	108 (55.6)
LCL–ELSh kt (m s^{-1})	80 (41.2)	37 (19.0)	70 (36.0)	40 (20.6)	43 (22.1)	21 (10.8)	101 (52.0)	71 (36.5)
0–ELSh kt (m s^{-1})	81.6 (42)	52.5 (27)	95.2 (49)	44.7 (23)	42.8 (22)	42.8 (22)	95.2 (49)	89.4 (46)
EBWD kt (m s^{-1})	49 (25.2)	38 (19.5)	77 (39.6)	38 (19.5)	49 (25.2)	37 (19.0)	55 (28.3)	69 (35.5)
BRNSh (m^2 s^{-2})	89	50	196	34	56	56	25	80
T sfc ˚F (˚C)	80 (26.7)	79 (26.1)	78 (25.6)	81 (27.2)	86 (30)	65 (18.3)	70 (21.1)	81 (27.2)
Td sfc (˚F)	66 (18.9)	70 (21.1)	69 (20.6)	70 (21.1)	67 (19.4)	93 (33.9)	67 (19.4)	67 (19.4)
T 500 hPa (˚C)	–11.0	–14.5	–10.0	–10.7	–10.7	–10.0	–11.8	–10.0
FZL ft (m)	14 199 (4327.9)	11 819 (3602.4)	13 936 (4247.7)	11 903 (3628.0)	14 163 (4316.9)	14 778 (4504.3)	13 435 (4095.0)	14 258 (4345.8)
–10˚C ht ft (m)	18 540 (5651.1)	15 500 (4724.5)	18 676 (5692.5)	17 236 (5253.6)	18 775 (5722.7)	19 102 (5822.4)	17 830 (5434.5)	18 795 (5728.6)
–30˚C ht ft (m)	27 480 (8375.9)	23 993 (7313.1)	26 663 (8126.9)	25 884 (7889.4)	27 592 (8410.0)	27 735 (8453.6)	28 038 (8546.0)	28 546 (8700.8)
THK_{HGZ} (m)	2724.8	2588.7	2434.3	2635.8	2651.4	2631.3	3111.6	2972.2
GRWα_{EL}	–9.9	15.5	1.8	9.5	44.1	23.3	15.9	22.3
SRWα_{Mid}	111.4	97.9	125.9	99.9	119.4	96.6	99.7	126.5
LHP Term A	2.007	5.520	3.795	2.839	3.073	3.917	–0.276	1.164
LHP Term B	6.294	3.112	9.638	2.393	5.760	2.513	7.712	10.259
LHP	17.6	22.2	41.6	11.8	22.7	14.8	2.9	16.9
SHIP	1.7	4.0	2.6	1.7	2.5	1.9	1.0	1.4
SSP (m^3 s^{-3})	65 556	75 393	125 419	58 248	78 968	57 282	31 317	59 156
SCP	7.8	17.9	27.3	12.6	10.4	8.2	0.6	9.5

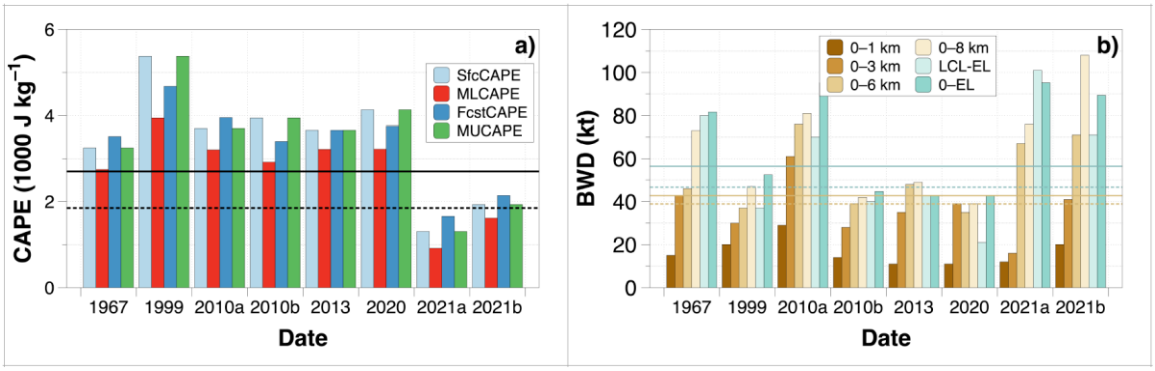

Figure 15: a) CAPE (1000 J kg^{-1}) and b) bulk wind difference (BWD; kt) shear values from observed and model-derived (NARR, NAMnest, and HRRR; Table 2) soundings for ≥3-in (7.6-cm) hail report dates in Cleveland County, OK, 1955–2021. In (a) black horizontal lines show MUCAPE thresholds of JS14: for ≥3.5-in (8.9-cm) hail, 2700 J kg^{-1} (solid) and for ≥2-in (5.1-cm) hail, 1850 J kg^{-1} (dashed). In (b), horizontal lines show shear thresholds proposed by JS14 for ≥3.5-in (8.9-cm) hail: 0–EL, 56.4 kt (29 m s^{-1}; solid aqua) and 0–6-km, 42.8 kt (22 m s^{-1}; solid khaki); and for ≥2-in (5.1-cm) hail: 0–EL, 46.7 kt (24 m s^{-1}; dashed aqua) and 0–6-km, 38.9 kt (20 m s^{-1}; dashed khaki).

All the Cleveland County ≥3-in (7.6-cm) hail date soundings had SHIP and LHP values sufficient to diagnose significant hail, except the April storm, which had SHIP of 1.0 and LHP = 2.9 [as noted previously, SHIP = 1.1 is the 10th percentile of the distribution for ≥2.5-in or 6.4-cm hail (SPC 2023f); JS14 LHP threshold for ≥2 or 5.1-cm hail is 5.0]. Furthermore, the SCP was only 0.6 for the April storm, whereas Thompson et al. (2004) show for surface-based supercells,the updated SCP of the 25th percentile is 2.2, which is satisfied in all the other cases. In the case of the April 2021 date, so many of the environmental sounding parameters might be considered marginal for significant hail that the occurrence of ≥3-in (7.6-cm) hail with this storm is quite perplexing. As we have shown, the interaction of the storm with regions that had 3+ in (7.6+ cm) of prior rainfall and possible associated baroclinic zones, interaction with the surface wind-shift boundary when the storm became close enough, the very large deep shear, as well as the small MLCIN values, all might help explain the significant hail sizes associated with the rapid intensification of the April storm.

Comparison of the radar reflectivity presentation and 60-dB*Z* reflectivity isosurfaces (Fig. 16) for each of the Cleveland County ≥3-in (7.6-cm) hailstorms (except for the 1967 case, for which radar data were unavailable) shows that all the cases were associated with isolated supercells, and that the 28 April 2021 storm was considerably smaller in areal extent than all of the others. The April storm's 2D radar reflectivity shows a stark contrast in morphology with the other ≥3-in (7.6-cm) cases. Only the April storm had a coherent (more than a few pixels) 70-dB*Z* reflectivity column (Fig. 16, special panel in right column, third row).

8. Summary and conclusions

We have presented case studies of two damaging hailstorms, both of which produced ≥3-in (7.6-cm) hail in Norman, on 28–29 April 2021 and 10–11 October 2021. We have also shown that hailstorms with ≥3-in (7.6-cm) hail in Oklahoma are rare, and that the occurrence of two such storms in a single year, in nearly the same location, is even more so.

The April storm formed well behind (≈60 mi or 96.6 km) a surface wind-shift boundary and intensified rapidly while nearing the surface wind-shift/convergence boundary at about 0100–0115 UTC 29 April 2021, ≈30 mi (48.3 km) west of the center of Norman, which may have provided enhanced lift. At this time, the storm showed an increase in maximum reflectivity to ≥70 dB*Z*, the development of a deep WER and well-defined inflow notch, an increase in mid-level rotation, and polarimetric signatures consistent with very large hail. Another possible contributing factor to this rapid intensification was the interaction of the storm updraft with a baroclinic zone and associated horizontal vorticity in the region of prior rainfall.

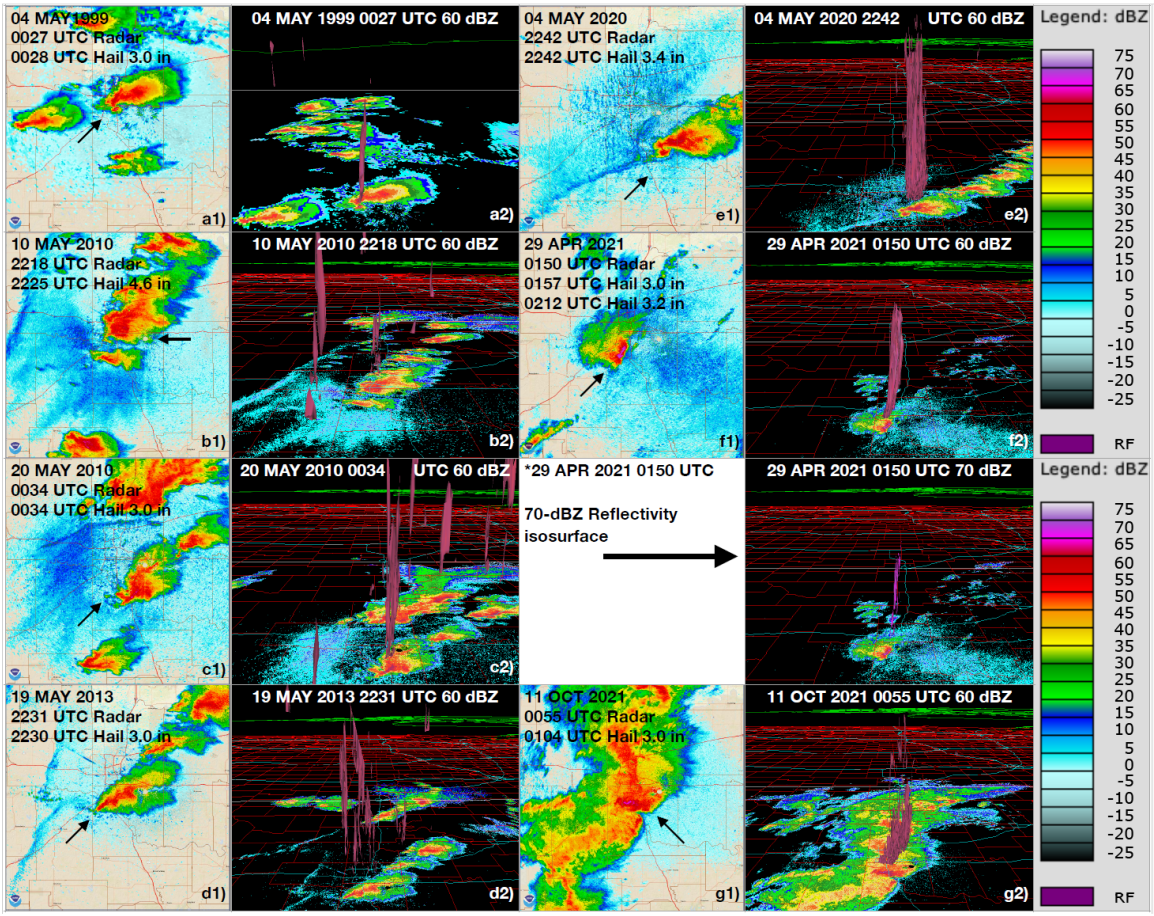

Figure 16: Radar reflectivity (first and third columns; panels denoted with a1, b1, etc., in lower right–hand corner) and 60-dB*Z* reflectivity isosurfaces (second and fourth columns; panels denoted with a2, b2, etc.; east direction is to the right) for each of the Cleveland County, OK ≥3-in (7.6-cm) 1955–2021 hailstorms (except for the 1967 case, for which radar data were unavailable). The unlettered panel in the right column, third row, shows a second 29 April 2021 isosurface plot, but with 70 dB*Z* at 0150 UTC. This was the only case with a coherent (more than a few pixels) 70-dB*Z* isosurface. In the 2D radar reflectivity panels, the first line of the title is the radar volume-scan date and time, and the second line (and third line for 28–29 April 2021) is the date and time of the maximum- (or two largest-) size hail report(s) within Cleveland County, OK. *Click image to enlarge.*

Moreover, for the April storm, the environmental model-derived sounding from KOUN exhibited marginal hail-related sounding parameters (lower values of CAPE, SHIP, LHP, etc.), but the deep shear values were large compared with published thresholds for wind-related parameters associated with significant hail. The occurrence of 3-in (7.6-cm) hail in such an environment begs the question of what other factors might have tipped the scales toward significant hail. When considering hail-size potential for storms in environments with low–moderate CAPE, consideration of large deep shear, interactions with boundaries, and regions of prior rainfall with possible associated baroclinic zones might be important to assessing potential changes in storm intensity and hail size.

The occurrence of ≥3-in (7.6-cm) hail in the fall (off-season or second-season) is also quite rare, which makes the October storm well worth documentation. This storm exhibited a more classic supercell morphology, had a history of tornadoes, evolved in an environment with larger (but still moderate) buoyancy, larger SRH, and large deep shear, all of which are storm and environmental characteristics more typical of springtime. Why the environment was more spring-like in mid-October is beyond the scope of this study, but the October case is a reminder

that significant hail events can occur anytime the environment is supportive, which can be overlooked in the off-seasons.

Upon comparison with the environments of the other (prior to 2021) six ≥3-in (7.6-cm) hail dates since 1955 for Cleveland County, the two 2021 dates were characterized by the lowest buoyancy, but some of the largest deep-shear values. The results support the idea that shear and/or buoyancy can, compensate for lower values of the other in the production of significant hail (provided the values are sufficient to sustain a supercell), and the association of long hodographs with significant hail (e.g., NA22 and others).

Ongoing work includes the consideration of the environments of other ≥3-in hailstorms within a larger area within Oklahoma. A reviewer (R. E. Jewell) noted that the environment of the second-costliest hailstorm in Texas, which occurred on 12 April 2016 and affected San Antonio, had many similarities to those of the two 2021 Norman storm dates. A goal of future research could include efforts to better estimate the potential for large hail in modest CAPE environments with long hodographs, through the identification and study of commonalities in a large number of such cases.

Limitations of this study include uncertainties inherent in storm reports, the absence of an observed sounding at KOUN at 0000 UTC on 29 April 2021, biases inherent in model-derived soundings, and the small sample size of the 3-in (7.6-cm) Cleveland County hailstorms from 1955–2021, which formed the basis for a comparison with the two 2021 hailstorms of interest.

In conclusion, these two 2021 hailstorms that affected Norman both were isolated and long-lived, lasting more than 5 h and traveling more than 200 mi (322 km). The two hailstorms were somewhat distinctive in that the 28–29 April 2021 storm was located behind a surface boundary, had only marginally or moderately hail-favorable environmental characteristics, and was extremely damaging; that the October storm was out-of-season for a ≥3-in (7.6-cm) hailstorm in central Oklahoma; and that both storms affected nearly the same locations in a single year, and as such, prompted this case study.

ACKNOWLEDGMENTS

We thank Aaron Johnson for graciously answering questions related to the Large Hail Parameter (LHP), and for reviewing and contributing to the LHP calculation information in Appendix A. We extend our gratitude to Steve Ansari of NOAA-NCEI for support with the Weather and Climate Toolkit (WCT) software. Denea Sadler, Alison Petrone, Zach Rael, and Tonya Faires are gratefully acknowledged for permission to use their photographs. We thank Patrick Marsh (SPC), Matthew Elliott (SPC), and Doug Speheger (NWS) for clarifications regarding the 19 May 2013 Cleveland County, Oklahoma and the 06 May 2001 Norman, Oklahoma hail reports. Rich Thompson (SPC) and Jay Liang (SPC) made available various sounding data, and Monica Mattox, Collin Mertz, and Cole Hartman kindly provided Oklahoma Mesonet data and maps. Other map figures were generated using Datawrapper software and charts were generated using DataGraph software (https://www.visualdatatools.com/DataGraph/).

Finally, we thank the reviewers for very helpful and insightful comments which believe have helped to improve the manuscript.

APPENDIX A: Large Hail Parameter (LHP)

Large Hail Parameter (Johnson and Sugden 2014). Additional details provided by Aaron W. Johnson (personal communication):

The LHP is set to zero if the 0-6 km shear magnitude <14 m s^{-1} or MUCAPE <400 J kg^{-1}. Otherwise, the LHP is defined as,

LHP = (Term A * Term B) + 5

where,

Term A = TermA1 + TermA2 + TermA3
Term B = TermB1 + TermB2 + TermB3

and,

TermA1 = (MUCAPE – 2000)/1000
TermA2 = (3200 – THK_{HGZ})/500
TermA3 = (LR_{7-5} – 6.5)/2

TermB1 = ($Shear_{EL}$ – 25)/5
TermB2 = ($GRW\alpha_{EL}$ + 5)/20
TermB3 = ($SRW\alpha_{Mid}$ – 80)/10

Terms are defined as,

- Shear6 = 0-6 km AGL bulk vector shear magnitude (m s^{-1}). The wind at 10-m height (i.e., typically the lowest sounding level) is used as the 0-m wind.
- MUCAPE = CAPE of the most unstable parcel (J kg^{-1}), which is the parcel with the highest equivalent potential temperature in the lowest 500 hPa.
- THK_{HGZ} = thickness of the layer between –10˚C to –30˚C, hail growth zone (HGZ; m)
- $LR_{7–5}$ = 700–500-hPa lapse rate (˚C km^{-1})
- $Shear_{EL}$ = 0–EL bulk shear (m s^{-1}). The wind speed at the EL (MU EL) is calculated as the non-pressure-weighted mean wind speed in the 1500-m layer below the EL height (Rasmussen and Straka 1998). The wind speed at 10-m height (i.e., typically the lowest sounding level) is used as the 0-m wind speed. A simple subtraction gives the bulk shear. Thus,

  $Shear_{EL}$ =
  speed of the mean wind in the 1500 m below the MU EL – speed of the 10-m wind (or lowest sounding level)
- $GRW\alpha_{EL}$ = simple subtraction of the ground-relative EL wind direction (˚) minus the ground-relative 3-6 km mean wind direction (˚). The ground-relative wind direction at the EL (MU EL is used) is calculated as the non-pressure-weighted mean wind direction in the 1500-m layer below the EL height (Rasmussen and Straka 1998). The 3-6 km ground-relative mean wind direction is calculated as the mean wind direction in the 3-6 km layer. The wind direction at 10-m height (i.e., typically the lowest sounding level) is used as the ground-level wind direction. Thus,

  $GRW\alpha_{EL}$ =
  [direction of the mean wind in the 1500 m below the MU EL – direction of the 10-m wind (or lowest sounding level)]
  –
  [direction of the mean wind in the 3–6 km layer – direction of the 10-m wind (or lowest sounding level)]
- $SRW\alpha_{Mid}$ = simple subtraction of the storm-relative 3-6 km mean wind direction (˚) minus the storm-relative 0–1 km mean wind direction (˚). The storm motion is determined using Bunkers right-mover storm motion vector (Bunkers et al. 2014). In this case, the 0–1-km mean wind direction is found from taking the average of the wind directions between heights of 0-1 km. The wind direction at 10-m height (i.e., typically the lowest sounding level) is used as the 0-m wind direction. Thus,

  $SRW\alpha_{Mid}$ =
  [direction of the mean wind in the 3-6 km layer – direction of the storm motion vector]
  –
  [direction of the mean wind in the 0-1 km layer – direction of the storm motion vector]

Constraints:

i) If $GRW\langle_{EL}$ >180˚, then set the entirety of TermB2 = –10;

ii) If TermA <0 and TermB <0 then LHP = 0; and

iii) If LHP = (TermA * TermB) + 5 is still negative after adding + 5, then set LHP = 0 to avoid ever having negative values of LHP.

Term A represents thermodynamic quantities and Term B represents wind-based quantities.

The strengths and weaknesses of the LHP are the following (A. Johnson, personal communication; quoted with permission):

"**Strengths**

- Designed to better delineate marginal supercell-based hail (e.g., ≈1.75–2.0-in) from giant hail (e.g., >= 3.5-in);
- Uses non-traditional inputs such as hail growth zone thickness that illustrate improved skill to differentiate between larger hail sizes compared to CAPE;
- Applies the shear and wind profile character above 6-km AGL to better discriminate between larger hail sizes compared to traditional severe-convective analysis using layers at or below 6-km AGL.

Weaknesses

- LHP does not illustrate much improvement in separating marginal severe hail from non-severe hail compared to traditional indices or composite parameters;

- Does not take into account duration of supercell mode or negative impacts on max hail size caused by anvil seeding from upstream convection;
- Values are not applicable with non-supercellular modes of convection such as a QLCS".

The LHP is a diagnostic and not a prognostic hail parameter, but with understanding of the limitations of such parameters (Doswell and Schultz 2006), might be able to be used with additional analysis to add to estimations of forecast hail size potential (Johnson and Sugden 2014).

APPENDIX B: Glossary of acronyms

CAPE	*Convective available potential energy*
CIN	*Convective inhibition*
MU	*Calculation using the most unstable parcel (parcel with the maximum equivalent potential temperature in the lowest 400 hPa)*
ML	*Calculation using the 100-hPa mean-layer parcel*
LCL	*Lifting-condensation level*
LFC	*Level of free convection*
EL	*Equilibrium level*
PW	*Precipitable water vapor below 400 hPa*
LowRH	*Mean relative humidity over the lowest 150 hPa*
MidRH	*Mean relative humidity over a layer 150–300 hPa above the surface*
ConvT	*Convective temperature*
SSP	*Significant severe parameter (Craven and Brooks 2004)*
LR_{7-5}	*700–500-hPa lapse rate*
LR_{8-5}	*850–500-hPa lapse rate*
SCP	*Supercell composite parameter (Thompson et al. 2007)*
SHIP	*Significant hail parameter (SPC 2023f)*
T 500 hPa	*Temperature at 500 hPa*
SRH	*Storm-relative helicity*
0–1SRH	*SRH from 0–1 km (Rasmussen 2003)*
0–3SRH	*SRH from 0–3 km (Rasmussen and Blanchard 1998)*
EffSRH	*Effective inflow-layer SRH (Thompson et al. 2007)*
0–xSh	*0–x km shear (bulk wind difference)*
LCL–ELSh	*LCL–EL wind shear (bulk wind difference)*
0–ELSh	*0–EL wind shear (bulk wind difference)*
EffSh	*Effective inflow-layer shear*
EBWD	*Effective bulk wind difference (Thompson et al. 2007)*
BRNSh	*Bulk Richardson number shear*
FZL	*Freezing level height*
xx˚C ht	*Height of xx = –10˚C, –20˚C, or –30˚C temperature*
THK_{HGZ}	*Hail-growth-zone thickness (layer between –10˚C and –30˚C; e.g., Nelson 1983)*
LHP	*Large hail parameter (Johnson and Sugden 2014)*
LHP Term A	*Buoyancy-related terms of the LHP(Johnson and Sugden 2014)*
LHP Term B	*Wind-related terms of the LHP (Johnson and Sugden 2014)*

REFERENCES

Allen, J. T., and M. K. Tippett, 2015: The characteristics of United States hail reports: 1955–2014. *Electronic J. Severe Storms Meteor.*, **10**, 1–31.

——, ——, and A. H. Sobel, 2015: An empirical model relating U.S. monthly hail occurrence to large-scale meteorological environment. *J. Adv. Model. Earth Syst.*, **7**, 226–243.

Balakrishnan, N., and D. S. Zrnić, 1990: Use of polarization to characterize precipitation and discriminate large hail. *J. Atmos. Sci.*, **47**, 1525–1540.

Bardsley, W. E., 1990: On the maximum observed hailstone size. *J. Appl. Meteor. Climatol.*, **29**, 1185–1187.

Blair, S. F., D. R. Deroche, J. M. Boustead, J. W. Leighton, B. L. Barjenbruch, and W. P. Gargan, 2011: A radar-based assessment of the detectability of giant hail. *Electronic J. Severe Storms Meteor.*, **6**, 1–30.

——, and Coauthors, 2017: High-resolution hail observations: Implications for NWS warning operations. *Wea. Forecasting*, **32**, 1101–1119.

Blumberg, W. G., K. T. Halbert, T. A. Supinie, P. T. Marsh, R. L. Thompson, and J. A. Hart, 2017: SHARPpy: An open-source sounding analysis toolkit for the atmospheric sciences. *Bull. Amer. Meteor. Soc.*, **98**, 1625–1636.

Brooks, H. E., and N. Dotzek, 2008: The spatial distribution of severe convective storms and an analysis of their secular changes. *Climate Extremes and Society*, H.F. Diaz and R.J. Murnane, Eds., Cambridge University Press, 35–53.

——, J. W. Lee, and J. P. Craven, 2003: The spatial distribution of severe thunderstorm and tornado environments from global reanalysis data. *Atmos. Res.*, **67–68**, 73–94.

Bunkers, M. J., and P. L. Smith, 2013: Comments on ‘‘An objective high-resolution hail climatology of the contiguous United States.’’ *Wea. Forecasting*, **28**, 915–917.

——, M. R. Hjelmfelt, and P. L. Smith, 2006a: An observational examination of long-lived supercells. Part I: Characteristics, evolution, and demise. *Wea. Forecasting*, **21**, 673–688.

——, D. Barber, R. Thompson, R. Edwards, and J. Garner, 2014: Choosing a universal mean wind for supercell motion prediction. *J. Operational Meteor.*, **2**, 115–129.

——, J. S. Johnson, L. J. Czepyha, J. M. Grzywacz, B. A. Klimowski, and M. R. Hjelmfelt, 2006b: An observational examination of long-lived supercells. Part II: Environmental conditions and forecasting. *Wea. Forecasting*, **21**, 689–714.

Craven, J. P., and H. E. Brooks, 2004: Baseline climatology of sounding derived parameters associated with deep moist convection. *Natl. Wea. Dig.*, **28**, 13–24.

Davenport, C. E., 2021: Environmental evolution of long-lived supercell thunderstorms in the Great Plains. *Wea. Forecasting*, **36**, 2187–2209.

Davis, C. A., and M. L. Weisman, 1994: Balanced dynamics of mesoscale vortices produced in simulated convective systems. *J. Atmos. Sci.*, **51**, 2005–2030.

Dennis, E. J., and M. R. Kumjian, 2017: The impact of vertical wind shear on hail growth in simulated supercells. *J. Atmos. Sci.*, **74**, 641–663.

Doswell, C. A. III, and E. N. Rasmussen, 1994: The effect of neglecting the virtual temperature correction on CAPE calculations. *Wea. Forecasting*, **9**, 625–629.

——, and D. M. Schultz, 2006: On the use of indices and parameters in forecasting severe storms. *Electronic J. Severe Storms Meteor.*, **1**, 1–22.

——, H. E. Brooks, and M. P. Kay, 2005: Climatological estimates of daily local nontornadic severe thunderstorm probability for the United States. *Wea. Forecasting*, **20**, 577–595.

Dowell, D. C., and Coauthors, 2022: The High-Resolution Rapid Refresh (HRRR): An hourly updating convection-allowing forecast model. Part I: Motivation and system description. *Wea. Forecasting*, **37**, 1371–1395.

Edwards, R., and R. L. Thompson, 1998: Nationwide comparisons of hail size with WSR-88D vertically integrated liquid water and derived thermodynamic sounding data. *Wea. Forecasting*, **13**, 277–285.

EMC, cited 2023: North American Mesoscale (NAM) Analysis and Forecast System characteristics. [Available online at https://www.emc.ncep.noaa.gov/emc/pages/numerical_forecast_systems/nam/NAM_2017.pdf.]

Gauthier, M. L., W. A. Petersen, L. D. Carey, and H. J. Christian Jr., 2006: Relationship between cloud-to-ground lightning and precipitation ice mass: A radar study over Houston. *Geophys. Res. Lett.*, **33**, L20 803.

Grant, B. N., 1995: Elevated cold-sector severe thunderstorms: A preliminary study. *Natl. Wea. Dig.*, **19**, 25–31.

Gutierrez, R. E., and M. R. Kumjian, 2021: Environmental and radar characteristics of gargantuan hail-producing storms. *Mon. Wea. Rev.*, **149**, 2523–2538.

Hales, J. E. Jr., 1988: Improving the watch/warning program through use of significant event data. Preprints, *15th Conf. on Severe Local Storms*, Baltimore, MD, Amer. Meteor. Soc., 165–168.

Heymsfield, A. J., and D. J. Musil, 1982: Case study of a hailstorm in Colorado. Part II: Particle growth processes at mid-levels deduced from in-situ measurements. *J. Atmos. Sci.*, **39**, 2847–2866.

Horgan, K. L., D. M. Schultz, J. E. Hales Jr., S. F. Corfidi, and R. H. Johns, 2007: A five-year climatology of elevated severe convective storms in the United States east of the Rocky Mountains. *Wea. Forecasting*, **22**, 1031–1044.

Iowa State University, cited 2023: Iowa Environmental Mesonet (IEM), rawinsonde (RAOB) data archive. [Available online at https://mesonet.agron.iastate.edu/archive/raob/.]

Jewell, R., and J. Brimelow, 2009: Evaluation of Alberta hail growth model using severe hail proximity soundings from the United States. *Wea. Forecasting*, **24**, 1592–1609.

Johns, R. H., J. M. Davies, and P. W. Leftwich, 1993: Some wind and instability parameters associated with strong and violent tornadoes: 2. Variations in the combinations of wind and instability parameters. *Geophysical Monograph Series*, C. Church, D. Burgess, C. A. Doswell III, and R. P. Davies-Jones, Eds., Vol. 79, American Geophys. Union, 583–590.

Johnson, A. W., and K. E. Sugden, 2014: Evaluation of sounding-derived thermodynamic and wind-related parameters associated with large hail events. *Electronic J. Severe Storms Meteor.*, **9**, 1–42.

Kelly, D. L., J. T. Schaefer, and C. A. Doswell III, 1985: Climatology of nontornadic severe thunderstorm events in the United States. *Mon. Wea. Rev.*, **113**, 1997–2015.

Kumjian, M. R., and A. V. Ryzhkov, 2008: Polarimetric signatures in supercell thunderstorms. *J. Appl. Meteor. Climatol.*, **47**, 1940–1961.

——, and K. Lombardo, 2020: A hail growth trajectory model for exploring the environmental controls on hail size: Model physics and idealized tests. *J. Atmos. Sci.*, **77**, 2765–2791.

——, ——, and S. Loeffler, 2021: The evolution of hail production in simulated supercell storms. *J. Atmos. Sci.*, **78**, 3417–3440.

Lin, Y., and M. R. Kumjian, 2022: Influences of CAPE on hail production in simulated supercell storms. *J. Atmos. Sci.*, **79**, 179–204.

MacIntosh, C. W., and M. D. Parker, 2017: The 6 May 2010 elevated supercell during VORTEX2. *Mon. Wea. Rev.*, **145**, 2635–2657.

Mesinger, F., and Coauthors, 2006: North American Regional Reanalysis. *Bull. Amer. Meteor. Soc.*, **87**, 343–360.

Moore, J. T., A. C. Czarnetzki, and P. S. Market, 1998: Heavy precipitation associated with elevated thunderstorms formed in a convectively unstable layer aloft. *Meteor. Appl.*, **5**, 373–384.

Morgan, G. M., and N. G. Towery, 1975: Small-scale variability of hail and its significance for hail prevention experiments. *J. Appl. Meteor.*, **14**, 763–770.

——, and P. W. Summers, 1982: Hailfall and hailstorm characteristics. Thunderstorms: *A Social, Scientific and Technological Documentary,* Vol. 2*, Thunderstorm Morphology and Dynamics*, E. Kessler, Ed., U. S. Government Printing Office, 363–408.

NSSL, cited 2023: MRMS (Multi-Radar Multi-Sensor) operational product viewer. [Available online at https://mrms.nssl.noaa.gov/qvs/product_viewer/.]

NCEI, cited 2023a: Storm events database. [Available online at https://www.ncdc.noaa.gov/stormevents/.]

——, cited 2023b: WCT radar visualization software. [Available online at https://www.ncdc.noaa.gov/wct/.]

——, cited 2023c: Storm events database, event details. [Available online at https://www.ncdc.noaa.gov/stormevents/eventdetails.jsp?id=956954.]

——, cited 2023d: Storm events database, event details. [Available online at https://www.ncdc.noaa.gov/stormevents/eventdetails.jsp?id=988176.]

Nelson, S. P., 1983: The influence of storm flow structure on hail growth. *J Atmos. Sci.*, **40**, 1965–1983.

Northern Illinois University, cited 2023: NIU Meteorology NARR (North American Regional Reanalysis) sounding generator. [Available online at https://atlas.niu.edu/narr/.]

Nixon, C. J., and J. T. Allen, 2022: Distinguishing between hodographs of severe hail and tornadoes. *Wea. Forecasting*, **37**, 1761–1782.

Nowotarski, C. J., P. M. Markowski, and Y. P. Richardson, 2011: The characteristics of numerically simulated supercell storms situated over statically stable boundary layers. *Mon. Wea. Rev.*, **139**, 3139–3162.

Ortega, K., 2018: Evaluating multi-radar, multi-sensor products for surface hailfall diagnosis. *Electronic J. Severe Storms Meteor.*, **13**, 1–36.

Picca, J., and A. Ryzhkov, 2012: A dual-wavelength polarimetric analysis of the 16 May 2010 Oklahoma City extreme hailstorm. *Mon. Wea. Rev.*, **140**, 1385–1403.

Rasmussen, E. N., 2003: Refined supercell and tornado forecast parameters. *Wea. Forecasting*, **18**, 530–535.

——, and D. O. Blanchard, 1998: A baseline climatology of sounding-derived supercell and tornado forecast parameters. *Wea. Forecasting*, **13**, 1148–1164.

——, and J. M. Straka, 1998: Variations in supercell morphology. Part I: Observations of the role of upper-level storm-relative flow. *Mon. Wea. Rev.*, **126**, 2406–2421.

——, S. Richardson, J. M. Straka, P. M. Markowski, and D. O. Blanchard, 2000: The association of significant tornadoes with a baroclinic boundary on 2 June 1995. *Mon. Wea. Rev.*, **128**, 174–191.

Schaefer, J. T., J. J. Levit, S. J. Weiss, and D. W. McCarthy, 2004: The frequency of large hail over the contiguous United States. Preprints, *14th Conf. on Applied Climatology*, Seattle, WA, Amer. Meteor. Soc., 3.3.

Smith, T. M., and Coauthors, 2016: Multi-Radar Multi-Sensor (MRMS) severe weather and aviation products: Initial operating capabilities. *Bull. Amer. Meteor. Soc.*, **97**, 1617–1630.

Snook, N., and M. Xue, 2008: Effects of microphysical drop size distribution on tornadogenesis in supercell thunderstorms. *Geophys. Res. Lett.*, **35**, L24 803.

SPC, cited 2023a: WCM page—Hail days. [Available online at https://www.spc.noaa.gov/wcm/climo/sighail.png.]

——, cited 2023b: Significant hail probabilities. [Available online at https://www.spc.noaa.gov/new/SVRclimo/climo.php?parm=sigHail.]

——, cited 2023c: Severe Weather Maps, Graphics and Data Page. [Available online at https://www.spc.noaa.gov/wcm/.]

——, cited 2023d: Preliminary local storm reports for 10 October 2021. [Available online at https://www.spc.noaa.gov/exper/reports/?date=20211010&hoursBefore&all.]

——, cited 2023e: Severe weather events archive. [Available online at https://www.spc.noaa.gov/exper/archive.]

——, cited 2023f: Significant Hail Parameter. [Available online at https://www.spc.noaa.gov/exper/mesoanalysis/help/help_sigh.html.]

Straka, J. M., D. S. Zrnić, and A. V. Ryzhkov, 2000: Bulk hydrometeor classification and quantification using polarimetric radar data: Synthesis of relations. *J. Appl. Meteor.*, **39**, 1341–1372.

Thompson, R. L., R. Edwards, and C. M. Mead, 2004: An update to the supercell composite and significant tornado parameters. Preprints, *22nd Conf. on Severe Local Storms*, Hyannis, MA, Amer. Meteor. Soc., P8.1.

——, C. M. Mead, and R. Edwards, 2007: Effective storm-relative helicity and bulk shear in supercell thunderstorm environments. *Wea. Forecasting*, **22**, 102–115.

——, R. Edwards, J. A. Hart, K. L. Elmore, and P. Markowski, 2003: Close proximity soundings within supercell environments obtained from the Rapid Update Cycle. *Wea. Forecasting*, **18**, 1243–1261.

University of Wyoming, cited 2023: Department of Atmospheric Sciences, upper air data. [Available online at http://weather.uwyo.edu/upperair/sounding.html.]

Witt, A., 1998: The relationship between WSR-88D measured midlatitude rotation and maximum hail size. Preprints*, 19th Conf. on Severe Local Storms*, Minneapolis MN, Amer. Meteor. Soc.

——, M. D. Eilts, G. J. Stumpf, J. T. Johnson, E. D. Mitchell, and K. W. Thomas, 1998a: An enhanced hail detection algorithm for the WSR-88D. *Wea. Forecasting*, **13**, 286–303.

——, ——, ——, E. D. Mitchell, J. T. Johnson, and K. W. Thomas, 1998b: Evaluating the performance of WSR-88D severe storm detection algorithms. *Wea. Forecasting*, **13**, 513–518.

Zhang, J., and Coauthors, 2016: Multi-Radar Multi-Sensor (MRMS) quantitative precipitation estimation: Initial operating capabilities. *Bull. Amer. Meteor. Soc.*, **97**, 621–638.

Zrnić, D. S., 1987: Three-body scattering produces precipitation signature of special diagnostic value. *Radio Sci.*, **22**, 76–86.

REVIEWER COMMENTS

[Authors' responses in *blue italics.*]

REVIEWER A (Ryan E. Jewell):

Initial Review:

Recommendation: Accept with minor revisions.

Summary and overall impressions: This study was enjoyable to read, contains plentiful data to chew on, and notes weaknesses in reporting/observation data when needed. While much of it focuses on how rare these hail events are for the specific area of Norman, OK (interesting, but probably a function of chance), the case studies presented are quite relevant. Not because of where or how often they hit a single area, but because:

1) These hail environments happen more often than one might think (more on that under "Misc. Remarks").
2) This study is well-timed with other recent (referenced) research,
3) There is much room for improvement in hail forecasting ("low-hanging fruit"),
4) It has never been easier to compile and process data, including large data sets (of which both SPC and forecasters there have plenty), with an assortment of tools including AI, machine learning/training etc.

I am pleased to see research aimed at these specific hail forecasting issues, which I have observed for years. When real-world observations and modeling are in agreement, it is an exciting time because you know improvements in forecasting and therefore public service are coming soon.

We appreciate the encouraging words and agree it is a time of rapid changes/improvements in forecasting and research. We thank the reviewer for these helpful and thought-provoking comments. We believe they have led to tightening up of certain arguments and improvement in the manuscript.

In addition to changes outlined in specific review responses, other changes to the manuscript include the following:

- *Fig. 4 made into 2-panel figures spanning four pages as suggested by Reviewer A.*
- *Fig. 5 added storm slinkies to the sounding diagrams*
- *Fig. 6 insets of low-level (0-2 km) rotation tracks were replaced with mid-level (3-6 km) rotation tracks from MRMS based on Reviewer B's suggestion and that mid-level rotation is more relevant to hail growth (e.g., Heymsfield and Musil 1982 showed that trajectories of the largest hail cyclonically traversed the periphery of the mid-level mesocyclone within the hail growth zone). Also, labels F-J instead of A-E were corrected on Fig. 6b rotation track inset. References to Fig. 6 insets were adjusted accordingly throughout the text. Corrections were made to the county name labels.*
- *Fig. 8 panels zoomed in for better clarity and surface boundaries adjusted slightly.*
- *Fig. 9 was revised to include vertically integrated liquid (VIL), vertically integrated ice (VII), as well as layer thicknesses of the 50-dBZ echo over 0 ˚C and 60-dBZ echo over –20 ˚C. Consideration of these quantities to aid in assessing storm intensity was suggested by Reviewer A.*
- *Fig. 12a replaced April BWER with a higher-level view*
- *Fig. 13 Radial velocity panels were removed for the following reasons: 1) We did not feel confident in the accuracy/precision of manually determined azimuthal shear values in the presence of folded velocities (for 0144 UTC 29 April 2021) and 2) more accurate rotation values were available from MRMS.*

Major Issues: No major issues with this case study

[Editor's Note: Although the reviewer categorized the comment below as "minor", we believe the question, suggestion and reply ultimately became substantive and impactful enough to include as part of the review record.]

Minor Issues and Questions: Introduction: You mention that the storm "was sub-severe until it approached the boundary", and I assume that means in terms of hail production. But I wonder, was the storm actually "weak overall" before it interacted with the boundary (in terms of echo tops, VIL, lightning, size), or, was it just that is started producing more/larger hail at that point? The former could be a question of lift, realizing instability, and getting the storm machination in place, while the latter could mean the storm-relative winds, and/or embryo source region(s) were modified. Please consider investigating and/or elaborating further.

Response to the second portion of the Reviewer's comment: We appreciate the reviewer's comment regarding the possible dynamical/physical processes that the storm might have undergone depending upon its level of severity at a given time (we agree these seem plausible), but evaluation/support for of these possible processes would require a more in-depth investigation of the storm dynamics, which is beyond the scope of the current paper. Nevertheless, consideration of the storm organization and hail formation mechanisms at various times in the storm lifecycle would indeed comprise an interesting future research study. However, we did further investigate/revisit the storm strength/severity, as described next.

We did mean that the April hailstorm was sub-severe, based on the fact that no severe reports (no reports at all; severe criteria are hail ≥1 in or 2.54 cm, and/or winds ≥58 mph or 25.9 m s^{-1}, and/or a tornado) had been received prior to 0134 UTC, but also based on the storm morphology appearance on radar (Fig. 11), storm rotation values (Fig. 6a inset), and other measures. The storm had mixed severe and non-severe characteristics at various times, but no severe hail reports until 0134 UTC 29 April 2021, and no severe thunderstorm warning until 0128 UTC 29 April 2021, when the storm was located near Amber, OK, in north-central Grady County. Just to be clear, we never imply that sub-severe equals "weak," although it could.

To address/further investigate the first question of the Reviewer's comment regarding storm strength, we have added to Fig. 9 (now included in the revised manuscript, the layer thicknesses of the 50-dBZ echo over 0˚C and the 60-dBZ echo over –20˚C, vertically integrated liquid VIL, and vertically integrated ice VII (VII related to lightning density; Gauthier et al. 2006). In addition, we revisited the other measures, including echo-top heights (original Fig. 9), maximum reflectivity (Fig. 10), storm size (Fig. 11), polarimetric variables (Fig. 13), already presented in the manuscript.

When re-examining the criteria for a severe thunderstorm [warning], we find that some thresholds, such as 50-dBZ echo tops >8 km (for a strong storm for which a severe warning might be appropriate, Lemon 1977) were satisfied as early as 0030 UTC 29 April 2021. Based on Donavon and Jungbluth (2007, their Table 1), the criterion would be a 50-dBZ echo-top height of 11.2 km, given a melting level of ≈4.12 km, (Fig. 5a of the current study shows FZL=13 435 ft or 4.1 km), and the only time where the 50-dBZ echo height = 11 km (no larger heights were found) based on 10-min sampling was at 0150 UTC. However, the 50-dBZ echo-top criterion performs best for weakly to moderately sheared environments for which weak-echo region (WER) and three-body scatter spike (TBSS) are better hail indicators (Donavon and Jungbluth 2007) and the April (and October) 2021 Norman, Oklahoma storm environment(s) was(were) highly sheared.

Consideration of vertically integrated liquid (VIL; Kitzmiller et al. 1995 state that VIL can be used to determine whether a storm is severe or not, but, Edwards and Thompson 1998 found VIL was not useful to discriminate hail size; now added to Fig. 9) showed values that roughly follow the trends of the 50-dBZ echo top height changes, while the VIL density only exceeded 3.5 kg m^{-3} (Amburn and Wolf 1997 criterion for severe hail) at one time when it was ~4 kg m^{-3}, 0120 UTC (not shown). Vertically integrated ice (VII, related to lightning density; Gauthier et al. 2006; now added to Fig. 9) values showed a rapid increase at 0120 UTC, consistent with the time of rapid intensification. Additionally, MESH values show one pocket of

hail size values >20 mm (0.79 in) in western Caddo County at about 0016–0018 UTC, prior to the more continuous >20-mm values starting around 0049 UTC (Fig. 6a).

The mid-level rotation criterion for the definition of a supercell of ≥0.01 s^{-1} was not satisfied for more than one 2-min interval (0104 UTC) based on MRMS, until 0120 UTC. A TBSS (not all times and elevations were checked; KTLX radar is used for information in this review response) was noted first, for one radar time, 0014 UTC, at 1.25˚ elevation, and then again at 0054 UTC (near the time of rapid intensification) at 3.03˚ elevation and in most scans thereafter, until the storm was past Norman. No WER/BWER was identified at 0014 UTC, but WER/BWER signatures were seen at ~0059 UTC at 1.71˚ elevation and thereafter, perhaps until ~0241 UTC at 3.91˚ elevation (not all times and elevations were checked).

From the MESH values, echo top heights, VIL, VII and layer thicknesses (new Fig. 9a,), as well as lowest elevation radar scans from additional times (not shown), a gradual intensity increase is evident starting around 0000 or 0014 UTC with some fluctuations in intensity, but the most rapid and larger increases occurred at around 0100 UTC (this rapid intensification is especially noticeable in VII values – thank you for suggesting examination of VII). The polarimetric signatures (Fig. 13) indicate that at 0029 UTC (during the more gradual increase) the hail signatures indicated much smaller hail over a smaller area than at 0144 UTC.

[Editor's Note: Figure added to paper is omitted here for space/redundancy considerations.]

Thus, the April storm could have been capable of severe hail prior to the first hail report at 0134 UTC (and perhaps prior to the severe warning at 0128 UTC), but enough metrics do not meet criteria normally associated with severe storms to make the severe status of the April storm questionable at times prior to about 0100 UTC (again we are not saying the storm was necessarily weak). Based on a synthesis of all of these metrics, and consistent with the MESH signature and rotation values (Fig. 6a), we conclude that the April storm may have been briefly severe from 0014–0016 UTC (pocket of ≥20 mm MESH, TBSS, and other measures but these were not sustained) while in western Caddo County, but decreased again to sub-severe levels, until about 0100 UTC, when it neared the surface wind-shift boundary in western Grady County.

- *Therefore, we have retained the statements that characterize the storm as "sub-severe" since the storm did not have severe hail or wind, nor tornado reports (nor a severe warning) until after the time of rapid intensification (~0100–0115 UTC 29 April 2021).*

- *We did add [a] statement regarding the brief pocket of larger MESH values.*

- *We also adjusted the description of the revised Fig. 9 to incorporate the additional data plotted.*

[Minor comments omitted...]

Second review:

Recommendation: Accept.

REVIEWER B (Aaron W. Johnson):

Initial Review:

Reviewer recommendation: Accept with minor revisions. No further review is requested unless major changes are made in accordance with other reviews.

Review Characteristics:
Overall Scientific Content: Good
The conclusions follow from the evidence: Very Good
The paper is free of errors in logic: Good

Findings reproducible: Good
Overall Organization: Very Good
Impact: Good
Writing: Very Good
Figures & Tables**:** Very Good
(Scale: Very Poor, Poor, Fair, Good, Very Good, Excellent)

Overview: This manuscript reviews various details of two separate very large hail (≥3-in) events that impacted the Norman, Oklahoma area in 2021. While the authors detail the fact hail of this size is not anomalous in the historical record for central Oklahoma, they also illustrate the climatological rarity of two very large hailstone events existing within a single calendar year across Norman. Further, one of these two occurred in October, despite no other events with hail of this size existing outside of April or May in the historical record. A review of environmental conditions details somewhat similar synoptic conditions with a positively-tilted upper trough over the Intermountain West/Southern Rockies while a front was noted over central Oklahoma. Sounding analysis details substantial shear and elongated hodographs with both events that is consistent with prior research. However, positive buoyancy was found to be marginal relative to prior findings although still sufficient for deep convection.

Examination of radar data reveal initially discrete cells in both cases. Further, the April event was more isolated along with exhibiting a marginal supercell structure compared to the October case that more clearly resembled a supercell before transitioning into a linear mode. Both radar-algorithm output along with polarimetric and radial velocity data detail typical large hail signatures along with mesocyclone-based features. Finally, a comparison of these two events relative to other cases found in the historical record for Norman is detailed with the main environmental difference being lower CAPE values with the 2021 episodes, especially in the April event. Additionally, all storms were found to be associated with supercellular storms although the April 2021 case was considerably smaller in areal extent.

Overall, I have numerous but only minor comments to provide as the bulk of the manuscript is sound. The minimal burden that does exist in this manuscript lies in the authors needing to expand on dry vs. wet hail impacts at multiple points when noting reflectivity value changes along with MESH output. Further, several instances are found with only partial reference to findings in other hail-based studies as this includes minimal reference to the full distribution of values when evaluating parameter performance. Revisions to accommodate these issues should leave the manuscript in good standing for publication.

We thank the reviewer for these very insightful and helpful comments which we believe have helped to greatly improve the manuscript. We very much appreciate your careful review and thank you for raising these points, as they were helpful in refining, correcting, and making more precise, the descriptions of the observations. We have addressed the comments as described below.

[Editor's Note: General "other changes" reply section identical to that for reviewer A is omitted here.]

[Numerous minor comments omitted...]